Spring 5-15-2020

Exploring Attacks and Defenses in Additive Manufacturing Processes: Implications in Cyber-Physical Security

Nicholas Deily

Washington University in St. Louis

McKelvey School of Engineering

Department of Computer Science and Engineering

Thesis Examination Committee:
Ning Zhang, Chair
Stephen Cole
Chiamaka Asinugo

Exploring Attacks and Defenses in Additive Manufacturing Processes: Implications in Cyber-Physical Security

by

Nicholas Deily

A thesis presented to the Graduate School of Arts and Sciences
of Washington University in partial fulfillment of the
requirements for the degree of

Master of Science

May 2020
Saint Louis, Missouri

Contents

List of Figures

Acknowledgments

I want to express my gratitude to the members of the review committee: Professor Ning Zhang, Professor Steve Cole, and Chiamaka Asinugo. Each of you has meant so much to my educational journey.

Nicholas Deily

Washington University in Saint Louis
May 2020

Dedicated to my parents.

ABSTRACT OF THE THESIS

Exploring Attacks and Defenses in Additive Manufacturing Processes: Implications in Cyber-Physical Security

by

Nicholas Deily

Master of Science in Computer Science

Washington University in St. Louis, May 2020

Research Advisor: Ning Zhang

Many industries are rapidly adopting additive manufacturing (AM) because of the added versatility this technology offers over traditional manufacturing techniques. But with AM, there comes a unique set of security challenges that must be addressed. In particular, the issue of part verification is critically important given the growing reliance of safety-critical systems on 3D printed parts.

In this thesis, the current state of part verification technologies will be examined in the context of AM-specific geometric-modification attacks, and an automated tool for 3D printed part verification will be presented. This work will cover: 1) the impacts of malicious attacks on AM using geometrically-modified 3D models, 2) a 3D part reconstruction approach from medical imaging scans, 3) a mesh alignment technique based on point set registration, designed to handle abnormal part geometries, and 4) an automatic error detection and defect visualization tool for comparing the geometric similarity of 3D printed parts to their intended geometries.

Chapter 1

Introduction

1.1 The Emergence of Additive Manufacturing

Additive manufacturing (AM), the collective term for manufacturing processes that form 3-dimensional (3D) objects by adding material a single layer at a time, has become a core technology for many industries in recent years. The process itself is relatively straightforward; a computer-generated 3D model is sliced into a series of layers which are printed sequentially and fused together to form 3D parts. Depending on the exact process, the formed layers generally range in thickness from a few micrometers to many millimeters. However, because of the overall versatility of this process, 3D printing is used in many industries, including automotive, aerospace, aviation, and healthcare [30]. The layer-by-layer approach used in 3D printing has allowed manufacturers to create intricate parts with geometries that simply cannot be replicated through traditional manufacturing means, such as subtractive manufacturing or molding. In the case of molding-based processes, part geometries are limited by the constraints of current molding technologies. And while significant improvements in these processes over the past few decades have allowed for higher degrees of part intricacy, the cost of this technology as well as the long time it takes to create new molds makes AM processes a superior choice for many applications, specifically in cases where production volumes are

very low, or when intricate geometries are required in a final part. Subtractive manufacturing processes on the other hand, such as CNC milling, produce excessive amounts of material waste due to the nature of the processes [27, 81]. On top of this, these processes lack the versatility to create certain complex internal geometric features in a single production step. As such, when designing a part with complex internal features, subtractive manufacturing may require additional production steps, or may require a single part to be produced in several pieces. In many instances, this method may not be suitable at all.

Here, the use of AM for use in designing one-off parts, and creating complex geometries will be further discussed:

1.1.1 Designing One-Off Parts

Designing individualized one-off parts in manufacturing is often required in two distinct scenarios. The first is in the research and development stage of a product design process, where prototypes are made. During this stage of the design process, many iterations of a single part with slight variations are often made for testing. Using AM processes, modifying a design is as simple as making the necessary changes to the model of the part, and printing the new version. For molding and subtractive manufacturing however, making these seemingly straightforward changes are not so easy. For example, if injection-molding were used as the part production method, a single part modification would require a completely new mold, which would take significant time to produce, and likely cost thousands of dollars [28]. For subtractive manufacturing on the other hand, a new manufacturing procedure may have to be implemented depending on the details of the modifications, and new tooling equipment

may be required. As such, AM saves time and money when it comes to designing and testing parts during research and development.

The second use of AM for producing one-off parts, is when the exact design of a product must be tailored for each individual use, or when a single model cannot meet the demands for all of its use cases. This is often seen in medically related applications, where individual parts must be tailor crafted for each patient, due to slight variations in patient measuring shapes and constraints (i.e. different bone shapes, or different wound formations).

1.1.2 Creating Complex Geometries

In many manufacturing scenarios, complex internal shapes must be made, or separate internal parts must be designed inside larger enclosed volumes. Most traditional manufacturing technologies are unable to handle these assignments. In the case of molding technologies, creating shapes with multi-directional cavities becomes increasingly costly and difficult, and creating different fixtures inside semi-enclosed or fully enclosed outer surfaces is impossible. While subtractive manufacturing techniques such as CNC milling are somewhat more versatile when it comes to this, they still are lacking in many of the aforementioned scenarios. An example of complex geometric internal features produced using AM is shown in Figures 1.1 and 1.2, wherein a rook was designed and printed with complex internal and external geometries, all in a single production step.

Figure 1.1: 3D Printed Rook

1.2 Impacts of Additive Manufacturing Technologies

Because of the afforded versatility in designing intricate details in parts, without the worry of additional production steps or high costs, AM technologies have led to a new paradigm in manufacturing applications. This affects every level of production from the design stages, to part manufacturing, to post production processing, and importantly, quality inspection. This has led to recent technological advancements in a number of fields where manufactures have been able to broaden the scope of their designs. For example, in the aerospace industry, engine components are now being made using AM technologies which has allowed for the incorporation of built-in cooling channels in the internal structure of these components. This alone has led to significant improvements in engine performance [49]. GE is using 3D printing in their new LEAP jet project to manufacture fuel nozzles which are five times

Figure 1.2: 3D Printed Rook Overhead

more durable than previous generation models [42]. This has also decreased the amount of welding required, since intricate internal details can be designed with fewer separate parts.

1.3 Problem Statement

As an industry, AM has seen dramatic technological improvements in recent years, with new printing processes and new materials being added regularly. It is estimated that over 50% of manufacturers rely on some form of AM technologies, and this is expected to further increase over the next decade [74]. The AM industry is positioned to grow from $9.9 billion in 2018 to over $40 billion in 2025 [74], driven by an increasing demand for customized part manufacturing.

However, with the added versatility AM processes have, comes a set of unique security challenges that must be considered. This becomes particularly important considering the number of safety-critical sectors that rely on AM technologies.

The rest of this paper will be structured as follows: Section II introduces how AM technologies are used in medicine, and the security concerns associated with AM . Section III explores related work on part verification procedures, and looks at the implementation of cyber-physical attacked parts intended to evade detection systems. Section IV introduces a novel attack detection system, and describes each step of the detection mechanism in detail. Section V shows the results of testing the attack detection system on models created in Section IV.

Chapter 2

Background

2.1 Additive Manufacturing Technologies

Additive manufacturing, also referred to as rapid prototyping or 3D printing, exists in a variety of different forms, based on several different material processing techniques. When this technology began to emerge in industry in the early 1980s, it was viewed as a quick yet crude method of producing parts, perfect for designing prototypes, but not fit for production [11]. This is where the name, "rapid prototyping" originated from, as it was viewed at the time as a technology that would only be used in prototyping. However since that time, this technology has grown tremendously, and its place in many industries and a variety of uses has been solidified.

The process of creating a 3D print can be broken down into 4 steps. The first is creating a model of a part in a computer aided design (CAD) modeling software, or 3D modeling software. There are many such softwares available for this, ranging from programs specifically for designing mechanical parts, such as SolidWorks, to 3D graphics editing software, such as Blender. The next step after the model has been designed, is converting it into a mesh. A

mesh in its simplest form is a series of 3D points, referred to as vertices, which are connected together to form a series of planes enclosing the volume of the part. Traditionally, the mesh is saved in .stl file format, for use in the next step of the process, however, the use of other file formats, such as wavefront .obj files is becoming more common. Next, the mesh is processed by a slicing software, where it converts the mesh into a series of ultra-thin slices, ranging from a few micrometers to several millimeters. Here, each slices slice describes the shape and tool-path for each layer that the 3D printer will print. This information is usually stored in G-code format. In the final step, this information is passed along to the printer, which then creates the part layer-by-layer from the slices. The process is depicted in Figure 2.1.

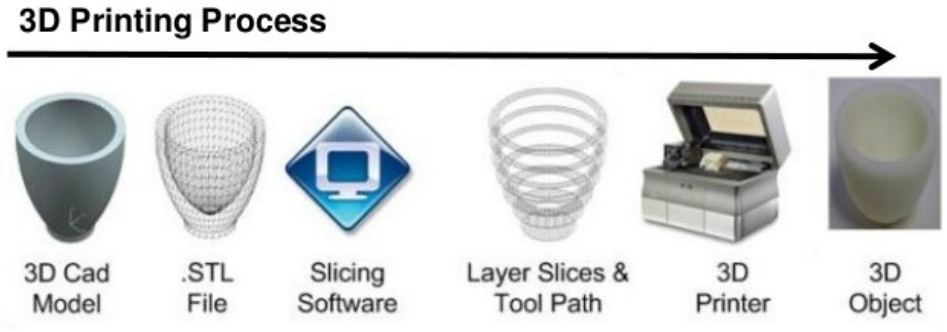

Figure 2.1: Steps in 3D Printing Process

While there are many forms of AM, the primary technologies can be grouped into 7 main categories; Material Extrusion, Powder Bed Fusion (PBF), Vat Photopolymerization, Material Jetting, Binder Jetting, Directed Energy Deposition, and Sheet Lamination. The following sections describe each processes in more detail.

2.1.1 Material Extrusion

Material extrusion, which includes Fused Deposition Modeling (FDM), and Fused Filament Fabrication (FFF), is the most common form of additive manufacturing. In this process, a

thermoplastic based filament is fed into a heated extrusion head, which deposits the material onto a build-platform layer-by-layer. The extrusion head is usually controlled by a series of stepper motors, and as such, the resolution of the printed part depends on the resolution of the motors, and the diameter of the extrusion nozzle. Generally the resolution of such printers is in the range of several hundred micrometers [51]. While this technology lacks the ultra fine-precision that other forms of AM have, and generally produces parts that lack mechanical integrity, [33], this technology is relatively affordable, and can produce complex geometries that are difficult to replicate through traditional forms of manufacturing. An example of a complex piece produced using this method this is shown in Figures 2.2 and 2.3:

Figure 2.2: FDM Bishop

For many shapes, extrusion printers rely on external support structures to provide support during the printing process, which can leave surface vestiges after they have been removed.

Figure 2.3: FDM Bishop Overhead

2.1.2 Powder Bed Fusion

Powder Bed Fusion (PBF) uses a high powered energy beam to melt or fuse material powder together to form a solid objects. The process works by dispensing a layer of powder, fusing selected areas together, lowering the entire printing bed, and depositing another layer of powder, repeatedly until the part is formed. Unlike Material Extrusion printing, there is no need for additional support structures, as the unfused powder is so tightly packed that it provides all of the support necessary as a part is constructed.

There are several forms of PBF, namely Selective Laser Sintering (SLS), Selective Laser Melting (SLM), and Electron Beam Melting (EBM), which are descirbed in further detail below:

1. **Selective Laser Sintering (SLS):** SLS uses a high power laser to heat areas of the powder, until they are hot enough to fuse together. In the sintering processes however, the material is not fully melted. SLS is primarily used with thermoplastics and metal alloys, and can form details on a nanometer scale [3,36]. An example of a complex part made using SLS is shown in Figure 2.4. This print contains several connected features that move in unison when the hand-crank is turned. All of these features however,

were printed together in a single print, and they were printed fully in their assembled state as shown.

Figure 2.4: Single PBF Nylon Print

2. **Selective Laser Melting (SLM):** SLM is a very similar process to SLS, except here, the material powder is fully melted before it fuses together, which results in different material properties than when the material is sintered. SLM is commonly used with pure metals and ceramic based materials [66].

3. **Electron Beam Melting (EBM):** EBM like SLM fully melts the powder material, however this process uses an electron beam in a vacuum chamber to melt the material, rather than a laser. This processes is often used with metals that oxidize easily [57]. Figure 2.5 show a hollow ball with a porous outer mesh made from a titanium alloy that was made using this processes. Notably however, another smaller version of the ball can be seen on the inside of the larger ball. The two objects are not connected in any way, yet they were printed in a single print.

Because of the nature of PBF processes, where powdered material is fused together, the material composition of of the powder can be adjusted from one area of a part to another.

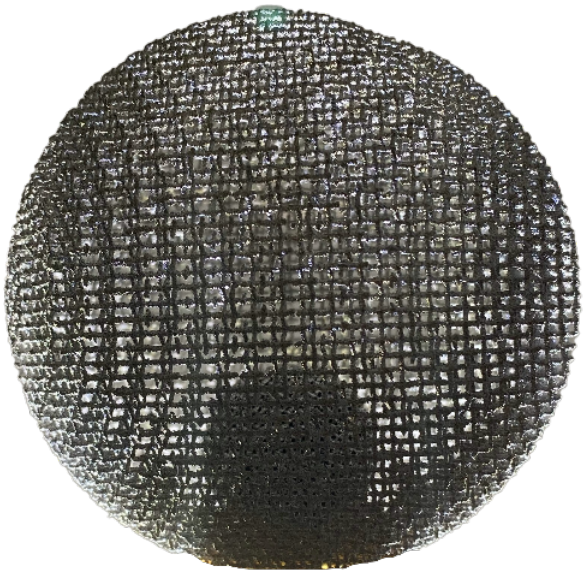

Figure 2.5: Single Print Concentric Titanium Spheres

Doing this allows for the creation of parts with material gradients [94]. This allows for objects to be made where material properties or alloy compositions are gradually adjusted throughout the volume of a part, simply by adjusting the material blend of the powder from one area to another.

2.1.3 Binder Jetting

Similar to the PBF processes, Binder Jetting uses layers of material powder, however it fuses the material together by dispensing a binding liquid in specific patterns for each layer, similar to how an inkjet printer dispenses ink [4]. Because Binder Jetting does not heat the materials to very high temperatures the way PBF processes do, its suitable for uses with materials that cannot be heated.

2.1.4 Material Jetting

Material Jetting processes dispenses tiny droplets of photocuring resin, which are then exposed to UV light which causes them to harden. Similar to Binder Jetting, Material Jetting dispenses material in a way very similar to how inkjet printers dispense ink. One of the advantages of this method is that multiple materials can be used in a single print, and easily mixed together, to form material blends [78]. As such, material properties can be easily adjusted from one region of a part to another.

2.1.5 Vat Photopolymerization

Vat Photopolymerization is the processes of selectively hardening a photocurable resin in a large tank. This processes generally uses an inverted build plate, that is slightly submerged into the liquid resin. From there, a focused source of UV light is shined in specific areas to harden the resin material, and cause it to adhere to the build plate. The bed is slightly raised, and the entire process is repeated for each layer.

In general, there are two types of Vat Photopolymerization techniques; Stereolithography (SLA), and Digital Light Processing (DLP), both of which are discussed in further detail below:

1. **Stereolithography (SLA):** SLA uses a UV laser to selectively cure regions of resin in the layers of a part [59]. This process can produce very intricate parts with very high levels of resolution. An example of level of complexity this process can produce is shown in Figures 2.6-2.11. In Figures 2.9 and 2.10, it can be seen that the rook and

bishop pieces have the same shape and internal complex structures as the full-scale pieces shown previously in Figures 2.3 and 1.2.

Figure 2.6: Micro SLA Chess Board Comparison

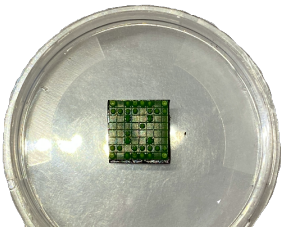

Figure 2.7: Closer Look at Chess Board

2. **Digital Light Processing (DLP):** DLP uses a screen to flash an image in the shape of each layer at the resin in order to cure it [37]. The resolution of this printing technique is limited by the size of the pixels comprising the screen, but this processes generally offers fast printing times, since entire layers can be formed simultaneously.

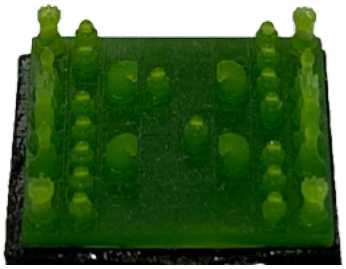

Figure 2.8: Chess Board 10x Zoom

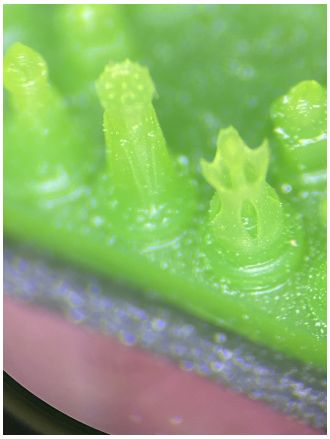

Figure 2.9: 75x Zoom Look at Bishop

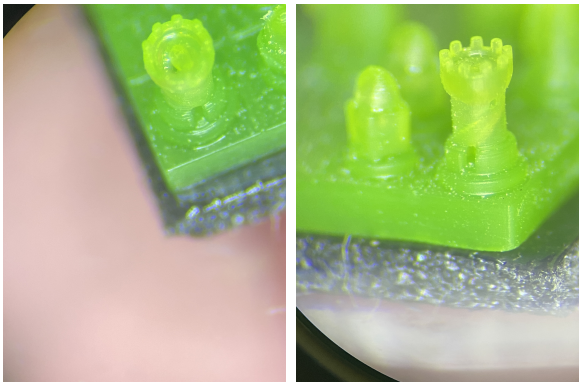

Figure 2.10: 75x Zoom Look at Rook

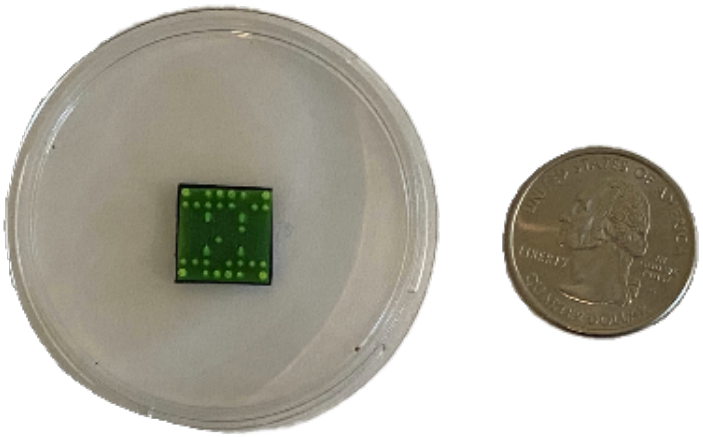

Figure 2.11: Chess Board Size Comparison

2.1.6 Directed Energy Deposition

This method is generally used with metals, where an extruder head extrudes a wire which is melted using a high energy laser, or electron beam [31]. As such, this process in many ways is a combination of FDM and PBF.

2.1.7 Sheet Lamination

Sheet lamination uses a processes whereby a thin layer of a material is stretched across a build surface, a shape corresponding to a layer geometry is cut out using a laser or milling tool, and the cut out material is then fused with the material underneath. A number of materials can be used in this processes, including a variety of polymers and metals [31].

The most common forms of Sheet Lamination are Ultrasonic Consolidation (UC), and Laminated Object Manufacturing (LOM).

1. **Ultrasonic Consolidation (UC):** UC uses ultrasonic vibrations to weld each layer of metal together, and form a single piece.

2. **Laminated Object Manufacturing (LOM):** Depending on the material substrate, LOM processes use heat and pressure, or adhesives to bind successive layers together to form a solid part [2]. This process is relatively inexpensive, but parts created using this method generally lack in structural integrity compared to other AM processes, such as PBF.

2.2 Medical Applications of Additive Manufacturing

One of the primary sectors that has shown interest in AM technologies, is the medical industry. The uses for AM in medicine are many; from dental prosthetics, to surgical guides, to anatomical models, to customized drug delivery vehicles. AM in medicine has found a number of niche uses due to its inherent flexibility and customizability, which is often needed to suit the needs of individual patients. Compared to traditional manufacturing techniques, AM processes provide a relatively fast and inexpensive solution for medical practitioners looking to design individualized parts. Where traditional manufacturing techniques may be better suited for the large-scale production of medical devices, AM processes are well suited for a number of medical scenarios, where treatments, surgical applications, or implants must be tailored specifically for each patient. These scenarios are discussed in greater detail below:

2.2.1 Surgical Guides

One area where 3D printing has drawn interest from the medical community is in the use of designing surgical guides. Surgical guides are used in many operations, a few of which are detailed below:

1. **Total Knee Replacement Surgery:** Total knee replacement (TKR) surgeries commonly rely on two types of surgical guides; pinning guides, which are used as an alignment tool, and cutting guides with designated slits meant to align femoral cuts [45]. The post-operative success of TKR operations depends largely on a near-perfect surgical accuracy during the procedure. In this type of operation, a coronal misalignment of as little as 3 degrees is associated with increased patient discomfort, and even knee replacement failures [17] as a result of abnormal force distributions on the knee [39]. The overall success of these operations has been greatly improved through the use of 3D printed surgical guides, which are custom printed to specifically fit each patient.

2. **Dental Guides:** AM plays an important role in dentistry where it is used to design drilling guides, as well as well as crown copings and bridge structures [Interactivedesign, 3Ddentistry]. Traditional methods of manufacturing these guides relied on vacuum forming, which often resulted in dimensional inaccuracies [41]. However, with AM technologies (particularly stereolithography) dentists have been able to base models off of highly accurate radiological and visual 3D scans, improving the accuracy and production times in these guides.

The exact shape and geometry of surgical guides must be customized for each patient in a highly specific manner. As mentioned above, the absolute accuracy in designing these

surgical aides is critical in most applications. With the ability to transfer patient specific data from medical imaging data to designs ready for direct printing, AM has helped streamline the process of designing these tools and supports. Additionally, due to the high cost of alternative manufacturing procedures for designing these tools [6], AM technologies offer a lower cost alternative. As a result of these advantages, doctors have been turning more and more to 3D printing as a solution to generate patient-specific parts. In particular, the use of stereolithography (SLA), has been widely adopted, due to its relative ease of use and low-cost of operation. Further, this printing technique offers a variety of readily available bio-compatible resins for part design [75].

2.2.2 Implants

The advent of medical printing technologies has allowed for the development of new treatments for patients based on customizable implant options. Bone implants in particular have benefited significantly from this technology, as doctors are able to design well-fitting bone structural supports to provide mechanical support and aid in repair processes. These developments have relied largely on powder bed fusion (PBF) printers, which are able to print solid metal, namely, titanium alloys, which are widely used in bone-repair applications. As such, doctors are using this technology to print a variety titanium-alloy based bone support structures, some of which are detailed below:

1. **Cranial Implants:** Injuries to the skull, arising from blunt force trauma, tumors, or in some cases, surgeries, result in structural damage to the cranial region. When the affected area is too large, the bone layer is unable to regenerate naturally, and as such, reconstructive surgery using structural implants is required in order to assist

in the natural restoration and reintegration phases [13]. The advent of selective laser sintering (SLS), and high temperature laser sintering (HTLS), has allowed doctors to work directly with titanium-based alloys, which has been shown to be best suited for these types of applications [15, 25]. This is mostly due to the structural rigidity and lightness of titanium compared to other materials. Additionally, this process has allowed for up to 85% reductions in total operation times, since doctors can simply attach the implant without the need to refine the shape of the implant during the operation, as was needed with traditional methods where titanium meshes were used. An example of a printed cranial implant is shown in Figure 2.12

Figure 2.12: 3D Printed Cranial Implant

2. **Hip Replacements:** While AM technologies are still being explored for use in designing hip-replacement features, preliminary studies on the use of this technology have been promising [64, 83]. The ability to design these parts to match the anatomical features of a patient, as well as incorporation specific porous microstructures on the surface of the implant to increase osseointegration makes this technology a promising solution for future applications in hip replacement surgeries [5, 35]. An Example of a 3D printed hip replacement part is shown in Figure 2.13.

Figure 2.13: Partial Print of Acetabular Hip Replacement Cup

3. **Bone Implants:** research is currently being done in order to analyze the possibility of using AM technologies in artificial bone replacement operations. Two important considerations that must be taken into account when constructing a bone implant, the mechanical properties of target tissue, and the fit between tissue and implant surface junctions. Traditional implants use solid metal pieces, which can result in stiffnesses of more than an order of magnitude greater than the target tissue [56, 92]. Using AM, the porosity of implant structures can be adjusted to closely match the mechanical properties of the target bone [47, 70]. Furthermore, the ability to modulate the shape and size of pores through AM plays an important role in osseointegration of the final parts [21, 73]. While titanium is the primary substrate used in most AM bone applications, other biodegradable materials are being researched [44].

2.2.3 Anatomical Models

One of the major uses of AM technologies in medicine is for the creation of anatomical models. Compared to traditional manufacturing techniques, it is relatively easy to convert medical scans into computerized models ready for printing [12]. Further descriptions of the use of AM in these applications are discussed below:

1. **Pre-Operative Aides:** AM has proven useful in designing anatomical models for pre-operative steps in surgical procedures. Hip replacements are one of the most common surgical procedures for those suffering from hip arthritis. 3D anatomical models of patient-specific surrounding hip structures have been proposed for use as pre-surgical aides where they would serve to simulate certain steps in implant operation. The use of such aides has been shown to be beneficial, because it allows surgeons to test fit implants before the real surgery takes place [84].

2. **Implant Shaping Props:** Anatomical models are used pre-operatively for shaping procedures in maxillofacial surgeries [[12, 61]. A recent study using pre-operative anatomical models in mandible microvascular reconstruction showed significant reductions in active surgery times [46].

3. **Educational Props:** AM is allowing educators to print a variety of anatomical models based directly off of tissue scans [29]. This has been influential in the development of more accurate models, as well as the development of models based off of patient specific data for use in understanding diseases and tissue abnormalities [80].

2.2.4 Drug Delivery Vehicles

Additive manufacturing has found a use recently in improving drug delivery systems. The use of this technology has primarily been focused in three areas; specialized drug lattices for oral release oral drugs, personalized medicine applications, and longer-term controlled release drug implants. A further discussion of these technologies is listed below:

1. **Oral Release Pills:** AM based processes have shown the ability to deopsit drugs in specialized 3D lattices that influence how well these drugs dissolve in solution. Based on this approach, manufactures have been able to control factors such as dissolving times for orally taken drugs [65], which has recently led to the first FDA approved 3D printed drug, Spritam [26]. Further, newer microfabrication technologies have shown promising results for enhanced localized delivery methods [6], as well as for the construction of dual-release tablets [53].

2. **Personalized Medicine:** In this era of personalized medicine, more and more treatments are becoming individualized in terms of dosages and treatments combinations which can be optimized on a case-to-case basis. In order to produce such personalized treatments, researchers are turning to AM technologies, particularly forms of Material Jetting, for its ability to deposit highly accurate dosages of multiple drugs in a controlled manner [7].

3. **Implantable Devices/Therapeutic Scaffolds:** Implantable devices made of bioactive materials or made with bioabsorbable materials with incorporated drugs or antibiotics have drawn interest from the medical community due to their ability to sustain

the release of bioactive agents for extended periods of time [19]. This may be particularly useful for implants in order to prevent infections and release growth factors locally over long periods of time, while having minimal impacts on other tissues [14].

2.2.5 Tissue Engineering

One of the major emerging fields in medicine is tissue engineering. Tissue engineering focuses on growing tissues to repair or replace damaged tissue or organs. Many tissues are unable to regenerate tissue for wounds larger than a few centimeters, and instead form regions of scar tissue. Additionally, many organs (like the heart), are unable to perform regenerative processes at all. Promising results from early studies into tissue engineering applications have led to increasing interest in this field of study, particularly in the past decade. Many tissue types are being examined for use in this technology [55], as well as a variety of printing methods, and new combinations of biocompatible printing substrates. The use of AM technologies in tissue engineering are primarily focused on the ability to recreate the natural complex cellular support structures, known as the extra cellular matrices (ECMs). These structures provide support which allows cells to develop in 3D spaces. As such, one of the primary applications of AM technologies in tissue engineering involves the direct manufacturing of porous scaffolds. As mentioned above, recreating the ECM is an important first step in the tissue development phase for nearly any tissue, as this plays an important role in cell attachment and proliferation. Designing a well structed scaffold to mimic an ECM often requires complex pore morphologies to be recreated. As such, AM has emerged as a promising solution due to the wide number of bio-compatible materials that can be used for printing, and the ability to design high resolution porous shapes on a micrometer scale [24]. Traditional methods of scaffold generation face limitations in terms micro scale control over

pore sizes and shapes [48], and macro scale control over the overall shape of a part. Further, using these AM approaches, a variety of these technologies have shown promise in the ability to closely mirror native tissue ECM structural properties [76], and modulate cell interface behavior [34]. To meet the demands for this new set of medical applications, 3D printers designed specifically for handling cell-based materials are being developed, known as bio-plotting printers [72]. These printers aim to integrate the structural construction of tissue lattices using multiple materials [40, 72], with the direct incorporation of cells and growth factors into a single printing process [34, 50]. Already, bio-inks, containing cell cultures encapsulated in hydrogels are being developed and tested [60]. Based on advances in this area, it is likely the case that as this technology continues to evolve for use in tissue engineering applications, new design and printing processes will continue to be developed to meet these new and unique production demands [48].

Overall, the use of AM technologies in medicine are already far reaching, with much ongoing research and development taking place. As new treatments are developed and approved, particularly for implants, engineered tissue replacements, drug delivery vehicles, and personalized medicine, it is likely that AM technologies will become the primary technology for many medical applications.

2.3 Additive Manufacturing Security Threats

Because AM technology is becoming so widely used in safety-critical industries such as medical care, aerospace, and automotive, the issue of security in AM is a growing concern. Many 3D printers rely on open source code, or code that has been derived from open source projects. Keeping 3D printing software open sourced has helped with the rapid development

of this technology in its early stages. However, this has also given attackers the ability to easily search for exploits in 3D printer firmware. Moore et. al. demonstrated how commonly used static code analyzers could be used to identify vulnerabilities in a variety of 3D printers [54]. Further, since many 3D printers have been designed with networking capabilities, they are vulnerable to exploits targeting embedded computing systems [22, 43]. The overall vulnerable nature of 3D printers to cyber-attacks has been well documented [69, 91].

One of the major concerns over cyber-physical attacks on 3D printers is the ability of attackers to modify a part, while having these modifications go unnoticed. Belikovetsky et. al. demonstrated this specifically, in an attack on a 3D printed drone propeller, which was shown to ultimately lead to a mechanical failure of the drone while in mid flight [10].

In an effort to make AM widely accessible, much of the technology surrounding 3D printers has been made open source and designed to use commodity hardware, such as simple embedded controllers like Raspberry Pi's, or similar devices. While this has allowed the technology to quickly develop and spread, it has created many avenues for attackers to potentially exploit. In fact, for most of the advantages 3D printing has to offer over conventional manufacturing techniques, there are corresponding security concerns. Take for example the previously discussed versatility AM offers in creating parts. A single 3D printer can be used to create objects of many different shapes and functions. The same versatility that allows for this could also allow a malicious attacker to replace a part with a visually identical substitute that has built in physical defects, or a part that uses different materials. While Belikovetsky et. al. demonstrated this form of attack to compromise a hobby drone, the same attack principals could be applied to other 3D printed objects such as bio-printed organs or airplane components, which could lead to devastating results.

The potential for hackers to exploit AM systems is clear, and as industries continue to adopt this technology and use it for more and more applications, the potential for great damage from cyber-phsyical attacks is clear. In the future, it will not be enough to react to AM security threats retroactively. Unlike traditional cyber attacks, where remedying a security issue can be accomplished through developing a security patch, remedying a security issue in an AM system would not address the issue of the potentially modified parts that were made while the system was vulnerable. As such, the need for additional security measures are eminent. In particular, a way to assess the printed results of each print produced using an AM system.

2.4 Verification Techniques

In order to address the potential security threats posed to AM processes, a new paradigm in the part verification process must be developed and assessed. Unlike most traditional manufacturing techniques, 3D printed parts have the potential to be modified in unique ways during each print cycle. And, because many AM applications are used to create unique versions of parts with every print, a verification procedure must be devised that can verify the accuracy of each individual part. While there is ongoing research in this area, generally, AM verification methods can be divided into two categories, active sensing procedures, and post-production verification procedures.

Active sensing procedures aim to detect abnormalities in printed objects during the actual printing process. In this scenario, attacks are detected live, as they are happening. The advantage of these procedures are that they are able to halt the printing process before an attack can be fully realized, potentially saving time and printing material. The drawbacks of these methods are that they are not very reliable, and mostly limited to FDM printers [9, 16, 93]. While some machine learning based verification techniques have shown promise for general error detection, they are severely limited in most part verification applications,

as they require large data training sets based on accurate models and pre-determined errors [89, 90]. Additionally, many of these detection mechanisms are designed simply to detect defects on internal infill patterns, limiting their applicability for general error detection scenarios.

Post-production verification procedures on the other hand rely on imaging and measuring techniques to verify the accuracy of a part after it has been printed. These techniques are used in a variety of medical and manufacturing applications outside of AM, and include: Computed Tomography (CT), Magnetic Resonance Imaging (MRI), Coordinate Measurement Machine (CMM) analysis, Ultrasonic Imaging, and 3D Scanning. A few of these approaches are being explored for use with AM parts [71, 88]. The issue however is that while these techniques can be used to produce fairly accurate images and measurements from printed models, they primarily rely on manual detection to compare images or measurements to their intended values, which has been shown to be unreliable for these tasks [79]. The rest of this paper will discuss the challenges associated with detecting errors and defects in physically altered 3D printed parts, as well as the implementation of an automated detection system using CT imaging.

Chapter 3

Additive Manufacturing Model Attacks

This section will discuss types of attacks on 3D printed models that could be implemented, as well as impacts of such malicious modifications.

3.1 Types of Attacks

When considering the potential attacks applicable to AM processes, a successful attack can be identified as a series of modifications to the geometry or material composition of a part that pass through any postproduction verification procedure undetected. For this project, the focus will be solely on geometric modifications. In general, geometric attacks can be broken down into a three sub-categories: (1) additive material attacks, wherein additional material is added to a part, (2) subtractive material attacks, wherein regions of the part are removed, and (3) geometric replacement attacks, wherein the design of a part, or region of a part is modified to affect the function of a part. A further discussion of each of these three attack categories is presented below:

3.1.1 Additive Material Attacks

1. **Surface Encroachment:** In this attack model, the physical boundaries describing the shape of a part are modified so that additional material is added around the

boundaries. This form of attack can be applied to almost any geometry, or subset of any part geometry. However, its realizable affects depend largely on the intended purpose of the part. A number of potential attack scenarios and potential impacts are listed below:

- Contracting the diameter of a hole in a PBF printed part intended for industrial application. This kind of malicious modification could range in impact from interfering with the minimum tolerance on a hole, to changing a fluid flow in a fluid-dynamic application, such as modifying the flow in part of a microfluidic device.
- Expanding the outer surface of a part beyond its physical specifications. The implications of this attack depend largely on the intended application of the part, but could range from causing an incorrect fit in a final assembly, to causing critical failures in a mechanical system.
- Modifying the pore size in a 3D printed tissue-scaffold, by adding material throughout the surface of each pore. The affect of this attack in particular could have serious health related implications, as such an attack could affect cell motility within a porous scaffold, leading to poor bio-related integration of a particular tissue. Similarly, even if cell motility were not impacted, such an attack could effect nutrient diffusion throughout the porous scaffold, leading to impaired cell growth or even death in certain regions of a part.

2. **Added Geometric Fixtures:** This attack relies on the addition of geometric features designed specifically to alter the functionality of a part, or affect defect detection mechanism in the post-manufacturing phase of the part cycle. The exact implementation of this attack would depend largely on the parts used in a physical system, however a few examples are listed below:

   - Added internal geometry in a tissue engineering application. Here, the presence of a mass in a tissue-engineered scaffold could serve to inhibit nutrient flow in a porous scaffold or serve to inhibit blood flow in a printed artery or vein. The implications of this could lead to tissue failure.
   - Masking other modifications. Depending on the part verification method present, the addition of particular geometries could serve to visibly mask other underlying

modifications that have been implemented in the geometry of a part. This could affect visual scanning systems, based on automated image matching from 2D image segmentation. Such an attack may be particularly impactful as such systems are often used in production settings.

- Filling an intended hole in an industrial application specific part. Here, an intended feature could be wholly erased from a part, leading to issues with integration of that part in specific implementations.

3.1.2 Material Removal Attacks

1. **Surface Thinning:** This attack implies just the opposite of the above-mentioned surface encroachment attack. Here, material is taken away along the surface boundaries of an entire part, or simply limited to specific regions of a part. This attack in particular among other things could detrimentally affect the mechanical properties of a part, or region of a part, leading to mechanical failures when under load. A number of attack scenarios are listed below.

    - Dilating a diameter in a hole in a part intended for industrial production, leading to issues with tolerancing, and potentially part failure.
    - Reducing wall thickness of a tubular section in an AM part, leading to eventual part failure from decreased wall shear strength.
    - Increasing the pore size in a bio-printed scaffold, leading to reductions in cell adhesion ability, and overall poor tissue viability, in the whole or subset region of a scaffold. In particular, this attack could be difficult to detect in sub-surface regions of the part.

2. **Geometric Fixture Deletions:** This attack relies on wholly or partially removing regions of a part. The effects of such an attack could be detrimental for many industrial applications, as well as medical specific applications. A summary of attacks falling under this category are listed below:

    - Removing a subsection of a bio-printed scaffold. Such an attack could wholly remove a region of scaffold, both affecting the mechanical properties of the part as a

whole, and affecting overall bio-incompatibility and cellular viability, particularly if the region was large enough to inhibit cellular motility.

- Removing layer subsets in a part. Due to the layer-by-layer approach in the process of creating AM parts, modifications can be on a layer-by-layer basis. And since any industrial AM printers can operate with layers on a sub-millimeter scale, attacks removing parts of layers at different intervals may be difficult if not impossible to detect, since most detection mechanism operate on a scale nearly an order of magnitude larger than this. Such an attack could affect the material properties of a part as a whole, particularly the shear and tensile strengths, leading to eventual failure depending on the application.

3.1.3 Geometric Substitution Attacks

Here, a geometric fixture from a part is modified from its originally intended shape, and function. This type of attack covers some of the most difficult to detect, yet most detrimental attacks in AM parts, due to its ability to appear to match the intended geometry of a part yet offer many differences in terms of physical functionality and mechanical properties. A number of example scenarios are detailed below:

- Modified pore morphology in a tissue scaffold. Here, the shape, direction, or interconnectivity of the pores in a porous scaffold could be modified to influence cell attachment, cell motility or even nutrient flow. And due to the random structure of many pore morphologies, such an attack would be very difficult to detect.

- Feature repositioning. Here, a feature such as a hole in a part could be moved so as to affect the part implementation in its final assembly. Such an attack may be difficult to detect unless a fully comprehensive measurements were taken post-production.

3.2 Attack Models

In order to test different attack scenarios against the proposed error detection mechanism presented in the next section, models based on a human trachea, a bone scaffold, and an orthopedic screw were selected. From here, multiple versions of each model were designed to implement a number of different attacks. The design process for each set of models is described in further detail below:

3.2.1 Trachea Model

A human trachea model provided by Professor Jammalamadaka Uduay from the Washington University School of Medicine in St. Louis was used as a base model, without any added modifications. This model is shown in Figure 3.1.

Figure 3.1: Trachea Model

This model was printed using FDM, using a Hyrel System 30M printer.

3.2.2 Bone Scaffold Models

The next model chosen was a bone scaffold. This model was chosen due the high degree of geometric complexity associated with such parts, along with the random nature of the structures, that make detecting changes to them a challenge. As discussed in previous sections, scaffolds play an important role in tissue engineering applications, as they provide

support for cell attachment and growth, similar to the way an ECMs do native tissues. As with most scaffolds, the pore size, interconnectivity, and shape play an important role in allowing for cellular attachment, motility, nutrient diffusion, and waste removal during the development stages. The bone chosen for this application was a thumb proximal phalanx bone, shown in Figure 3.2.

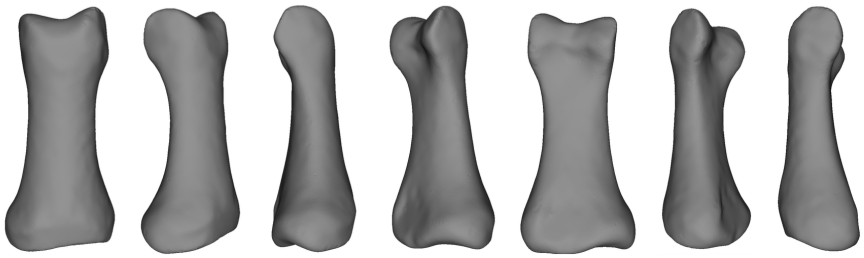

Figure 3.2: Thumb Proximal Phalanx

As mentioned earlier, 3D models or CAD models are comprised of 3D points, known as vertices, connected together to form series of triangles or quadrilaterals. Together, these triangles or quadrilaterals form surfaces which define the shape of a 3D object. Shapes described this way are collectively known as meshes. Because of the nature of how these shapes are modeled however, there are many different combinations of vertices and triangles/quadrilaterals that can form a single shape.

Because of this phenomenon, in many cases, mesh objects can be simplified, with minimal or even negligible losses to the spatial information of the model. This simplification procedure is referred to as decimation, or remeshing, and is an important step when dealing with large meshes. In the case of the bone model, the original mesh was comprised of over 19,000 vertices, and 39,700 triangles. Remeshing was done using Blender, a free-to-use 3D graphics editing software. A series of remeshed models were produced, containing a range from 4,000 triangles to 35,000 triangles. A model containing 20,000 triangles, or just over half of the traingles in the original was chosen, due to its visual similarity, and its reduction in overall complexity. The reduction in complexity is an important step, due to the next step which increases the complexity of a shape, in terms of total vertices by more than an order of magnitude.

The decimated model was loaded into Cinama4D, another 3D editing software, where a porous texture was created using Proc3durale, a 3D shading tool. The resulting model is shown in Figures 3.3, 3.4, 3.5.

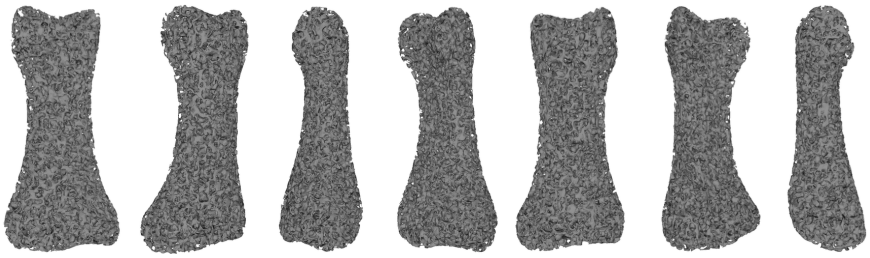

Figure 3.3: Porous Bone Model

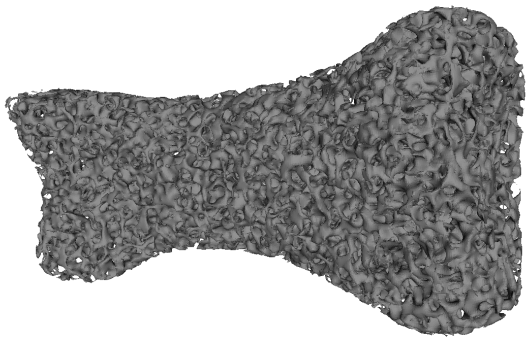

Figure 3.4: Porous Bone Model Close Up

From here, several attack models with modifications to this original design were created, to simulate different attack forms. A description of each is included below:

Hollow Internal Region Attack: Here, a series of 10 models were designed and created with three hollow internal spheres, spread throughout the internal regions of the mesh. The size of the internal spheres ranged in diameter from 500 micrometers, to 5 mm, with increments in size of 500 micrometers between each model. The purpose of this attack was to simulate a material removal attack, where a portion of the model was missing internally. The impacts of such a modification on a real-tissue engineering application could cause issue in cell viability due to the inability of cells to proliferate in the hollow regions.

Solid Internal Region Attack: Here, a series of 10 models were designed and created with three solid internal spheres, spread throughout the internal regions of the mesh. The size of

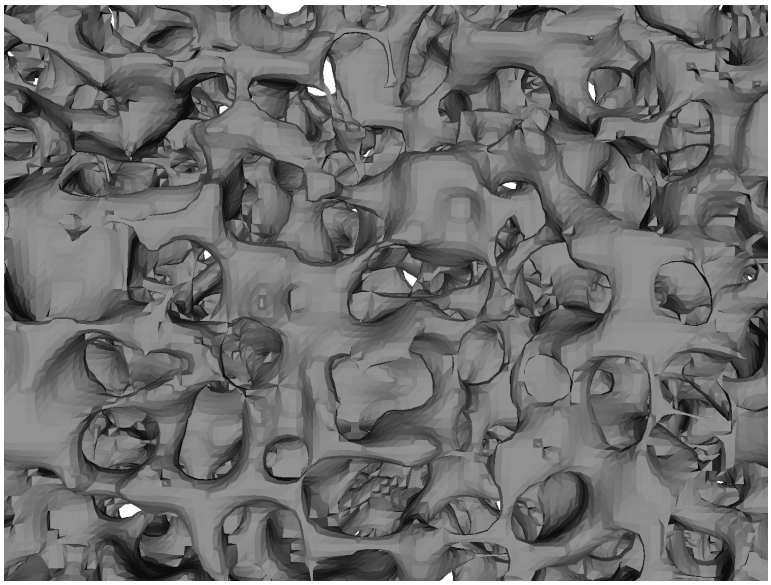

Figure 3.5: Porous Structure Detail

the internal spheres ranged in diameter from 500 micrometers, to 5 mm, with increments in size of 500 micrometers between each model. The purpose of these models was to simulate an additive material attack, wherein region of the bone were filled with solid material.

Modified Porosity Internal Region Attack: Here, 10 models were designed with an cylindrical internal region with a modified porous structure that was 2mm wide, and ranging from 300 micro-meters long to 6 mm long. The purpose of these models was to simulate a geometric substitution attack.

3.2.3 Bone Screw Model

The final model obtained, the bone is shown in Figures 3.6 and 3.7.

This model was modified by creating hollow internal region in the upper section of the screw. The purpose of this attack was to simulate a simple modification on such an implantable device, and simulate the detrimental effects that could result.

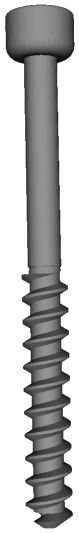

Figure 3.6: Bone Screw Model

Figure 3.7: Bone Screw Model Top

In order to perform this assessment, a finite element analysis (FEA) was performed on the original and the modified version of the screw, where a 100 N force was applied to a lower region of the model. The result of this analysis are shown in Figures 3.8 and 3.9.

The results indicate an increase in the stress in the attacked regions by more than an order of magnitude. The results were simulated with a relatively small force, considering its applications, and as such, its fair to assume such a modification could lead to mechanical failures if such an attack went undetected.

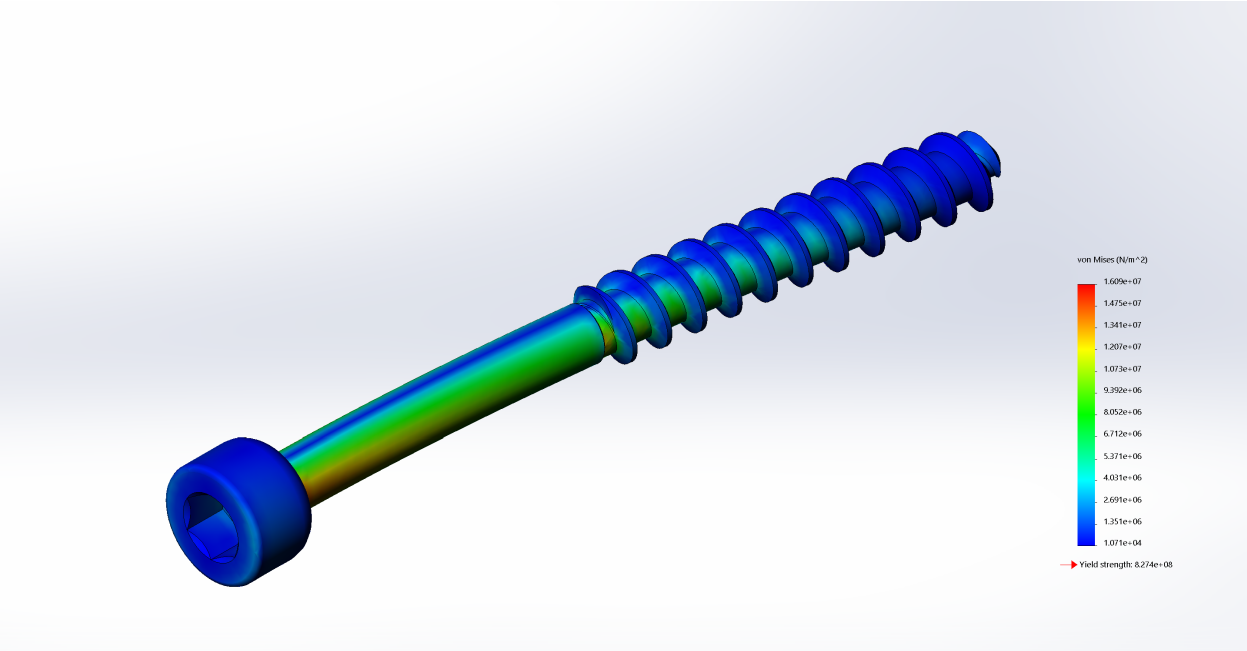

Figure 3.8: FEA of Original Bone Screw

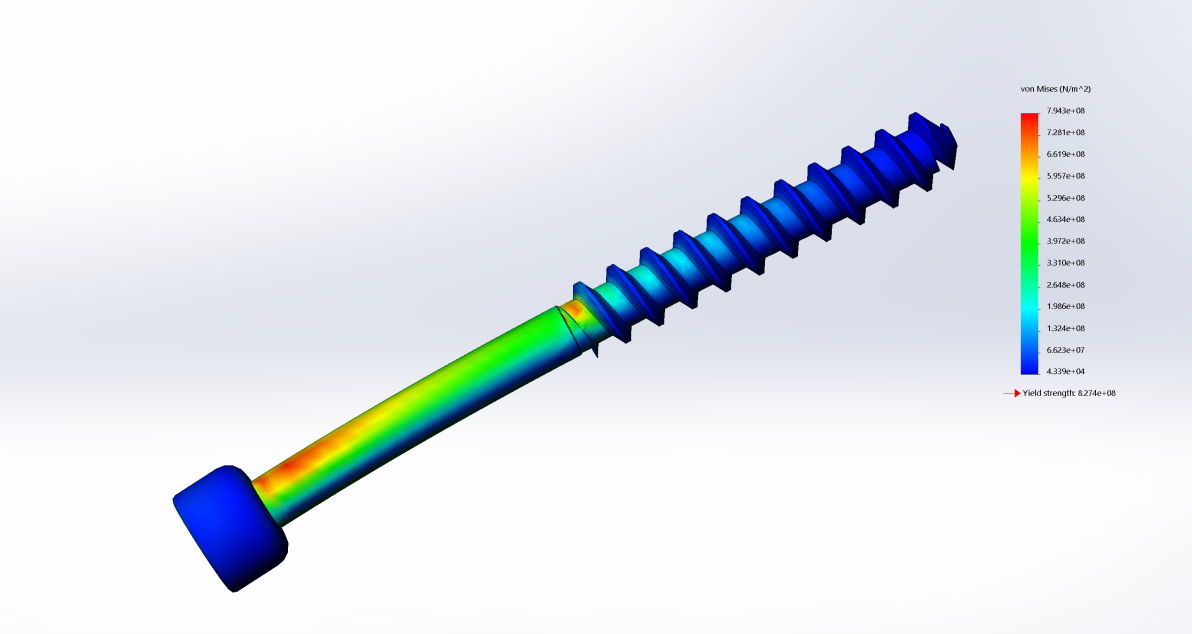

Figure 3.9: FEA of Modified Bone Screw

Chapter 4

Verification System Implementation

This section describes the implementation of an automated verification tool for comparing 3D printed parts to their intended geometries. The tool takes an input of CT scans of the printed part, along with its original 3D model, and performs a similarity comparison, wherein error regions are automatically detected and visualized.

4.1 Scanning

The first step in analyzing the accuracy of an AM part is generating a digitized 3D representation of its volume and composition. The method used for performing these measurements should ideally (1) capture a spatial representation of the part with a near perfect spatial-accuracy, (2) contain material-specific information throughout the entire volume, and (3) operate in a non-invasive and non-destructive manner, in order to preserve the integrity of the part. The technologies available for this are the previously mentioned passive part verification techniques; X-Ray Computed Tomography (CT), Magnetic Resonance Imaging (MRI), Coordinate Measurement Machine (CMM) analysis, Ultrasonic Imaging, and 3D scanning.

And as discussed in the previous section, due to a lack of surface penetration capabilities in CMMs and 3D scanners [23], and lower resolution outputs of Ultrasonic Imaging [85], CT and MRI technologies are superior choices for many part accuracy analysis applications. Choosing between MRI and CT depends largely on the material composition of the part in

question. MRI generally provides a higher degree of material differentiation for soft materials [67, 86, 87], but does not work as well with denser materials, due to shorter transverse relaxation times [52]. Alternatively, CT can provide a very high-level of resolution, particularly for denser materials [62, 63], but requires part exposure to ionizing radiation, which may be unsuitable in certain applications. For example, a tissue scaffold seeded with cells may be severely compromised if exposed to too much ionizing radiation. However, since no cell cultures were used in this experiment, CT was selected for the imaging procedure.

Modern CT scanners use a rotating emitter to project X-ray beams in a fan-shape towards multiple rows of detector arrays [32, 82]. An example of this is depicted in Figure 4.1:

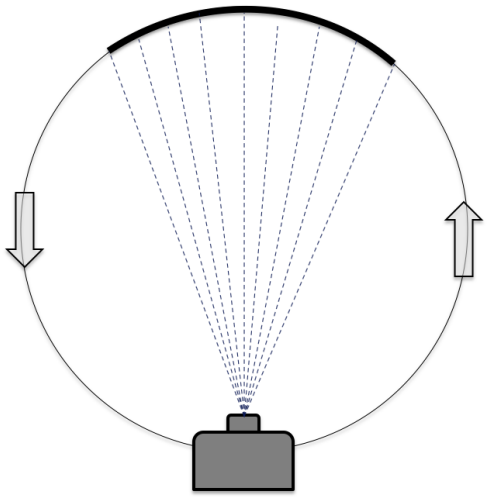

Figure 4.1: CT Scanner Diagram

In this setup, the apparatus rotates in a circular motion around the scanning subject, recording the X-ray signal intensities at each rotational position [38, 82]. The X-ray linear attenuation coefficients are then calculated for each volumetric unit (voxel) in the scanning volume and converted to Hounsfield Units (HU). These values, ranging from -1024 to 3071 are referred to as CT values, and generally correspond to the density of a material, with denser materials generally producing higher values [18]. However, even with modern day CT machines, scanning results are still be subject to some degree noise and image artefacts, which can lead to discrepancies between the CT values of voxels representing the same material in scan. This is particularly common for voxels near the surface boundaries of two different materials [77, 85]. Another source of noise is referred to as beam hardening, which occurs

when a material in a scanning volume over-attenuates lower energy X-rays. An example of this is shown in Figure 4.2, where a CT scan was taken of a patients head. In this image, some form of metal in the patient's teeth, likely in the form of a filling or crown caused significant beam hardening.

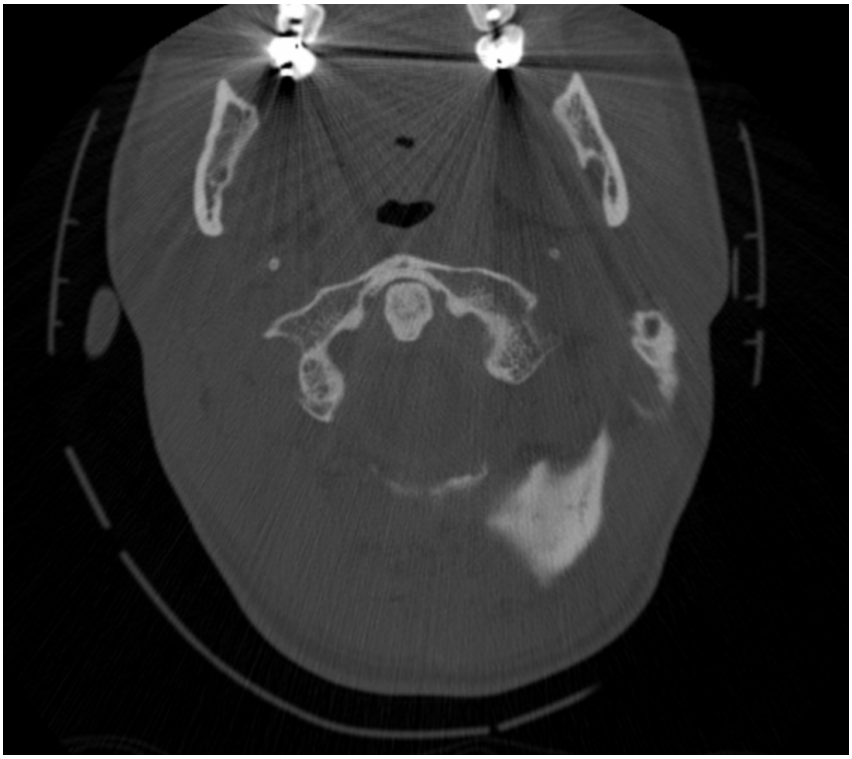

Figure 4.2: Beam Hardening Example

After the reconstruction process is complete, each axial slice in the scanning volume is converted into a 2D image, where every pixel in the image corresponds to a CT value in the volume. While the pixel data could easily be converted to grayscale values and exported as black and white images (as is done in some older CT machines), preserving the CT values plays an important role in volume processing steps. So instead, the images are stored in the Digital Imaging and Communications in Medicine (DICOM) format, where each image in this format contains a series of attribute tags encoding patient and scan specific information [1].

4.2 Object Reconstruction

Next, the processing step. The DICOM series contains tags specifying the layer thickness of each scan image, as well vertical and horizontal distances between the centers of neighboring pixels. Using this information, a digitized 3D representation of the scanning volume can be recreated by stacking the series along the scanning axis. Here, each voxel in the 3D representation corresponds to the CT-value observed in the original scan. Next, the set of voxels corresponding the AM part must be isolated. Ideally, this could be done by isolating the CT-value of the material of the AM part, and creating a subset of voxels containing only this value. In reality however, due to the aforementioned blurring and noise that results in inconsistencies in the recorded CT-values for voxels of the same material, the voxels of interest must be isolated from a range of CT values.

4.2.1 Marching Cubes Vs. Dual Contouring

Once the voxels corresponding to the part are isolated, this volume must be compared to the original CAD model of the part. The first step in this process is isosurfacing the voxel collection, to create a mesh representing the volumes of the part. There are multiple isosurfacing approaches, notably, Marching Cubes, and Dual Contouring. For this application, Dual Contouring was chosen, because of its ability to work with shapes with sharp features in the mesh reconstruction process [68], which is notedly an area that Marching Cubes is not well suited for. This reconstruction step produces a mesh representing the voxel volume of the scanned part.

4.2.2 Mesh Simplification

From here, the reconstructed mesh is simplified by removing overlapping triangles, and removing redundant faces from single planes.

4.3 Mesh Alignment

Next, in order to compare the reconstructed part to the original model, the reconstructed mesh (source mesh), must be spatially aligned to the original model mesh (target mesh). This is accomplished through two separate point registration steps, (1) global registration to roughly align the meshes, and (2) local registration to refine the alignment. However, in order to perform the alignment, distributed points from the surfaces of each mesh must be generated. Ideally, these point clouds should represent uniform surface samplings of each object. As such, the points describing the vertices are not suitable, due to their potential for highly irregular distributions. Instead each surface is sampled using Lloyd's algorithm to generate an evenly distributed set of point over the surface of each mesh. This process along with the registration procedures are described in further detail below:

4.3.1 Surface Sampling

In this step, a subset of surface points are taken from both the source and target meshes, which is needed to perform the alignment steps. This sampling procedure is important for complex meshes, given the computational complexity of the alignment algorithms makes it difficult to work with exceedingly large point sets.

In this sampling procedure, an initial subset of points are randomly selected from the surface of a mesh. These points are then used as generator points to form a Vonoroi diagram. Here, the surface is divided into a series of polygons, where every polygon encloses a single generator point in such a way that any position inside of a polygon is closer to its generator point than to the generator point of any other polygon. An example of such a diagram is shown in Figure 4.3:

After the initial diagram is formed, each point is migrated to the centroid of its polygon, and the points at these new positions are used as generators to form a new diagram. This processes is repeated iteratively until the generator points and polygon centroids converge from one iteration to the next. The results produces a distribution of evenly sized polygons, with points in the centroids of each. These points are then used the proceeding steps. This

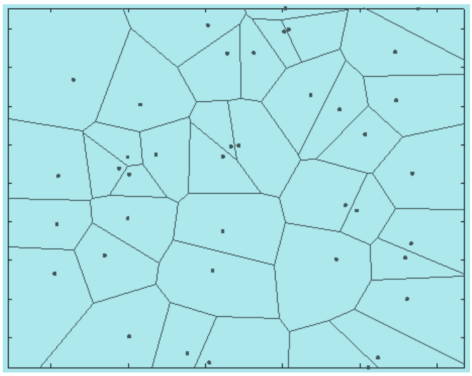

Figure 4.3: Example Voronoi Diagram

iterative procedure does not change the shape of the volume the sample points describe, but rather the distribution of the points over the surface of the volume.

4.3.2 Global Registration

Once the sampled points of each part have been obtained, the sampled points from the source mesh are coarsely aligned to the sampled points from the target mesh. This is done using a rigid transformation found from applying the Fast Global Registration (FGR) algorithm proposed by Zhou et. al. [95] to the two point sets. Next, the same rigid transformation is applied to the vertices of the source mesh, to coarsely align it with the target mesh. Transforming the vertices in the source mesh does not reorder the vertices in this mesh, which is important in preserving the geometry of the mesh.

4.3.3 Local Refinement

From here, the sampled points undergo a local rigid registration process using the Coherent Point Drift (CPD) algorithm proposed by Myronenko et. al. [58]. This was chosen over other local registration algorithms, notably Iterative Closest Point (ICP), because of its ability to work better with noisy point clouds [58]. This was an important consideration since this tool is intended to distinguished maliciously modified parts from their intended geometry,

and as such, must be robust enough to handle geometries that may introduce some form of noise to the sampled point sets.

From this process, the transformation found to align the sample point set to the target point set is then applied to the vertices from the source mesh, to further align it with the target mesh.

4.4 Similarity Comparison

Once the two meshes have been spatially aligned, a comparison procedure is conducted in two distinct steps: (1) comparing the source mesh to the target mesh to determine if there any added surfaces in the reconstructed part, and (2) comparing the target mesh to the source mesh to determine if there are any missing surfaces in the reconstructed part. Both steps are described in further detail below.

4.4.1 Comparing the Source Mesh to the Target Mesh

First, the distances from each vertex in the source mesh to their closest points in a target mesh are determined, in an operation where each point in the two meshes are compared.

Next, in order to identify geometric abnormalities between the two meshes, a subset of these vertices with distance values over a specified error threshold are isolated. The error threshold can be specified to any value, but in general, would depend on the tolerance of the part in question. From here, outlier points are removed from this isolated point set, based on proximity measurements to other points in the set, such that single outlying points are discarded. Then, the remaining points are segmented into clusters based on a specified threshold distance. This threshold depends on the size of the defect regions in question, such that, if the goal was to identify small defects, a lower threshold would be chosen, and if the goal was to detect larger error regions, a larger threshold would be chosen. Importantly, this step does not omit smaller errors even if a larger threshold is chosen. Instead, it simply determines the spatial size of individual defect groupings. Once this threshold has been set,

an automatic error detection procedure is conducted, where errors are identified based on the individual clusters formed.

Next, a for each point cluster, a minimum convex bounding volume is determined from a subset of the outermost points in the cluster. Then, the furthest distanced points in each convex hull are determined, and a sphere enclosing the point cluster is created.

Once the defect spheres for each point cluster have been determined, an adaptive wire-frame outline of the reconstructed mesh is rendered with the spheres overlaid on top, to visualize where the error regions occur.

Finally, the entire reconstructed mesh is rendered, with the colors of each point on the mesh corresponding to a color map based the previously calculated distances. This in effect produce a heatmap on the surfaces of the mesh.

From here, a slider tool is presented to which allows for the visual isolation of regions in the mesh corresponding to different levels of spatial divergence between the displayed source mesh and the target mesh. Adjusting the slider hides regions of the mesh based on their distance values, which allows for regions with greater distance values to be visually isolated.

4.4.2 Comparing Target Mesh to Source Mesh

Next, the target mesh is compared to the source mesh, in the using the same procedure described above. This is done in order to detect missing geometries in the source mesh. The reason this second procedure is done is because the distance determinations in the first step do not account for missing regions in the source mesh. In other words, if a region of the source mesh were missing, its likely the mesh would still align well with the target mesh, and the points that were present would not appear as defects. So in order to visualize missing regions in the source mesh, the target mesh must be compared back to the source mesh.

Chapter 5

Results

This section details results of the reconstruction procedure performed on CT scans of the trachea model, as well as geometric similarity comparisons performed on a the trachea model, the porous bone scaffold models, and the modified orthopedic screw.

5.1 Scanning Results

The CT scan of the printed trachea produced a series with 302 images. Samples throughout the volume are shown in Figure 5.1.

Here, the lighter pixels correspond with the higher CT values of the printed material, and the dark background pixels corresponded with regions outside of the printed volume. The images appeared fairly accurate, however, there was still some noise present, particularly around the edges of the object. The challenges associated with this are discussed in the following section.

5.2 Reconstruction Results

Since the part was made of a single material, the process of isolating the voxels that corresponded to the printed trachea involved separating those specific voxels from the voxels representing regions of air. In the first attempt to isolate the voxels corresponding to the

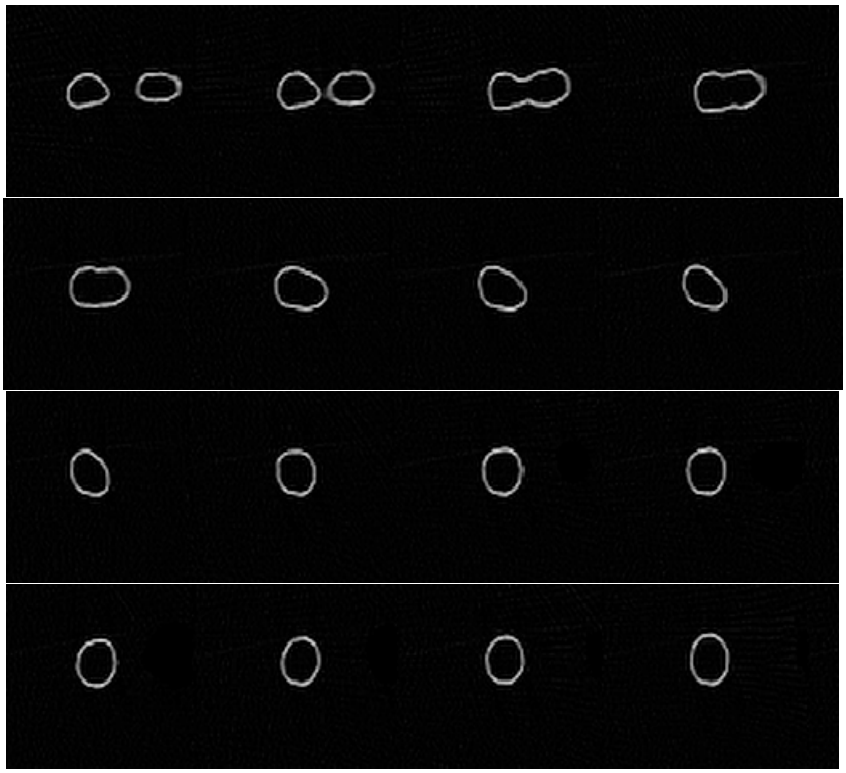

Figure 5.1: Samples of Scan Results

printed part, a range of voxels with CT values ranging from -220 to 100 were isolated. The resulting geometry is shown in Figure 5.2.

Figure 5.2: Initial Reconstruction Results

However, as is visually evident in the above figure, there were significant regions of missing material, particularly along the sides of the trachea. Additionally, this reconstructed volume

was visually inconsistent with the image sets as previously shown. However, a closer analysis of the voxel data made the issue clear; there were large regions of voxels representing the trachea that had very low CT values. Examples of this is shown in Figure 5.3, where top down slices of the voxel data have been rendered into a series of images.

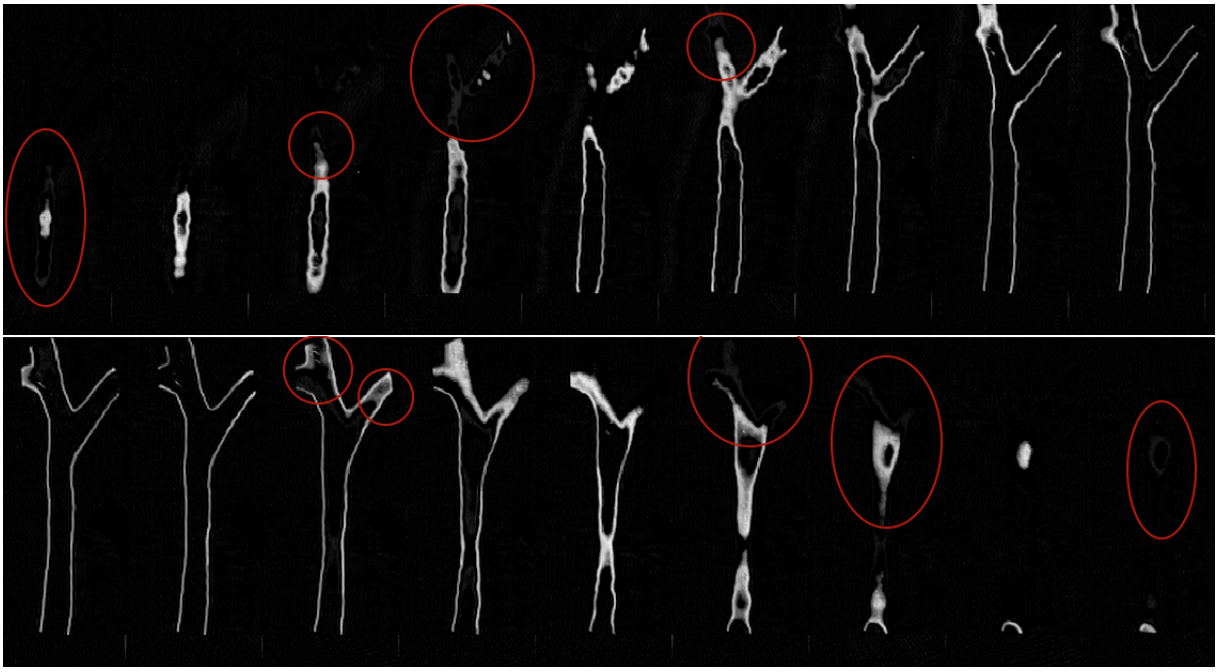

Figure 5.3: Inconsistent CT Values

From this, it was clear that a wide range of CT values represented voxels of the printed trachea. In order to account for this, the voxel sampling range was adjusted to isolate voxels with CT values from -720 to 100. The isolated voxels in this range are shown in Figure 5.4, and the results of the object reconstruction produced a reconstruction shown in Figure 5.5.

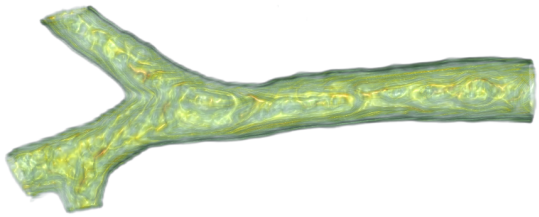

Figure 5.4: Isolated Region of Voxels

Figure 5.5: Full Reconstruction Results

In this scenario, increasing the CT value range was suitable, since the only material that the printed trachea needed to be distinguished from was the surrounding air, which had very low CT values of around -1000.

The initial reconstruction process yielded a mesh with 58473 vertices, and 116878 triangles, which was reduced to 17547 vertices and 35063 triangles after the automatic remeshing procedure.

5.3 Alignment Results

For the alignment procedure, a surface sampling of 2500 points was chosen for each mesh. The initial alignment of both samplings are displayed in Figure 5.6, where the red points correspond to the target mesh samples, and the black points correspond to the source mesh samples.

The alignment procedure was tested with and without the global registration step. In order to do this, the reconstructed mesh was randomly rotated before conducting alignment using CPD. This was done 100 times, which resulted in incorrect alignments 63 times. These poor alignments, are shown in Figure 5.7.

The same procedure was tested with the global registration step, which produced the correct alignment all 100 times. The correct alignment results are shown in Figure 5.8.

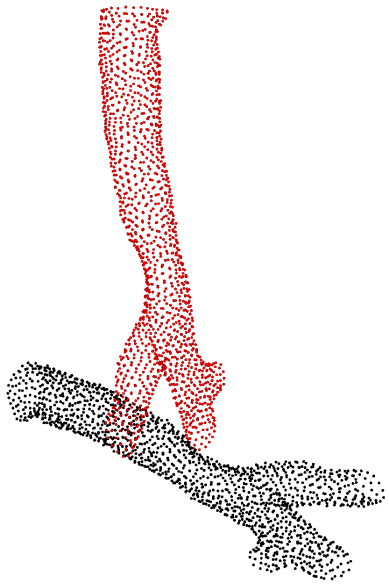

Figure 5.6: Initial Orientation

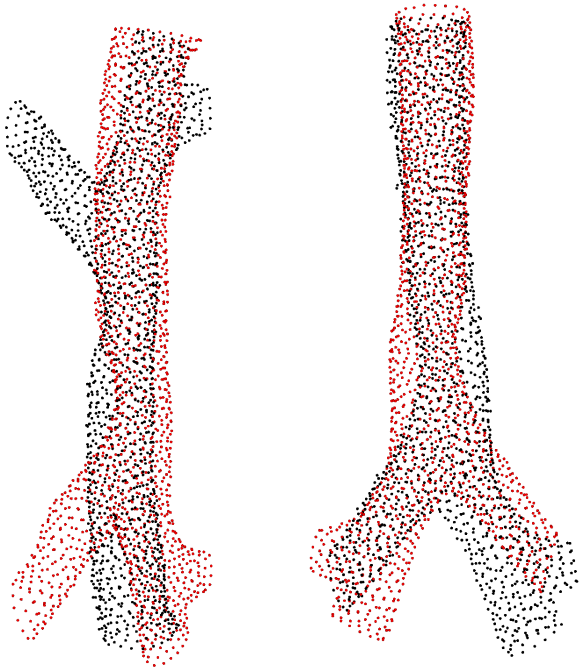

Figure 5.7: Alignment Issues with Only Local Alignment

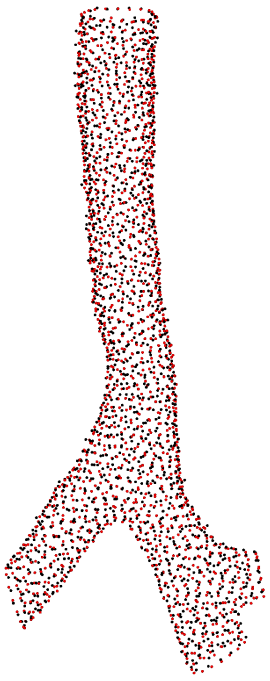

Figure 5.8: Proper Alignment

5.4 Comparison Results

5.4.1 Trachea Comparison

Once the transformations were determined from the registration steps, and the vertices in the reconstructed mesh were aligned with the original mesh. The similarity comparison procedure was conducted based on a tolerance criteria of 2 mm, and a defect grouping threshold of 6 mm. The results of the automatic error detection process are shown in Figure 5.9:

Next, the results of the visual heap-map representation are shown in Figures 5.10 and 5.11.

Finally, the use of the error isolation function is shown in Figures 5.12 and 5.13, where regions of the mesh are cut away until only segments corresponding to points with higher error values remain.

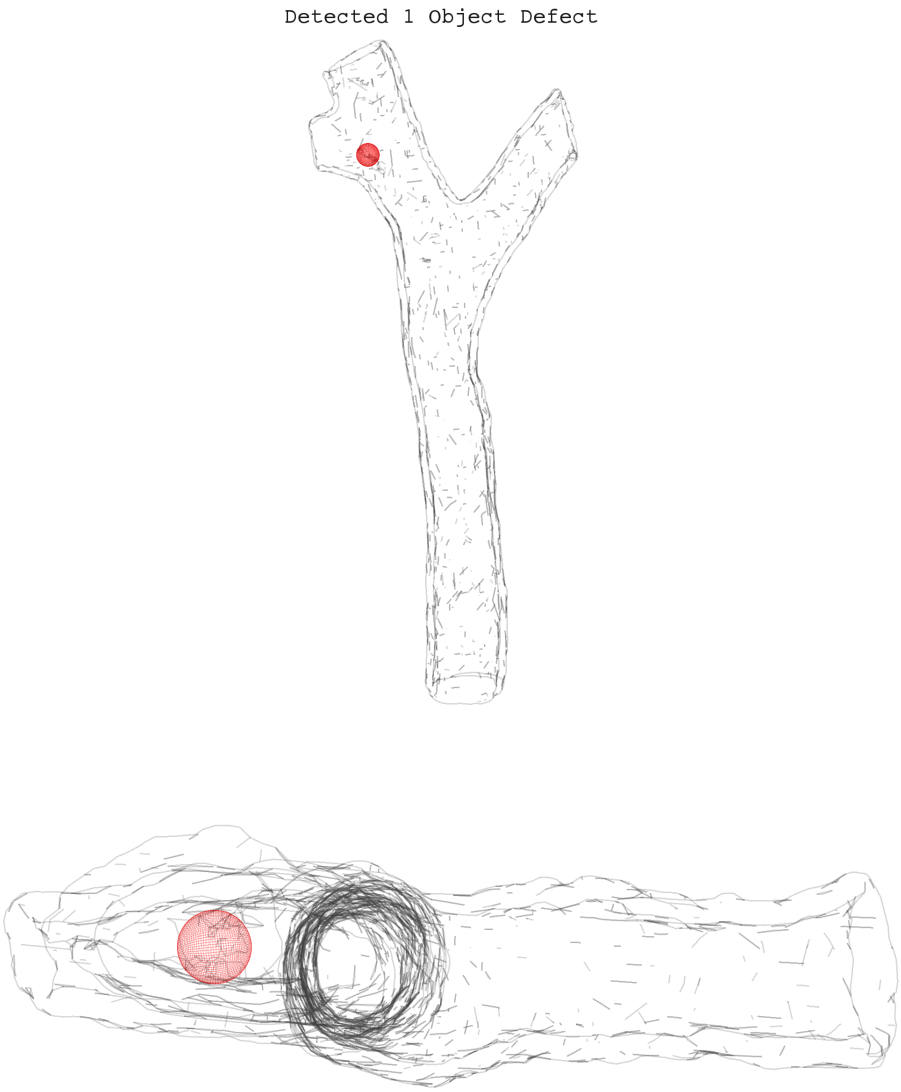

Figure 5.9: Automatic Error Detection

Next, the results of the comparison of the target mesh to the source mesh are shown in 5.14. Notedly, there were no errors detected in the automated error detection process, since the maximum divergence was about 1.7 mm, which was less than the error threshold of 2 mm. The region with the most divergence can be seen on the edge of the model, where it appears reddish in color.

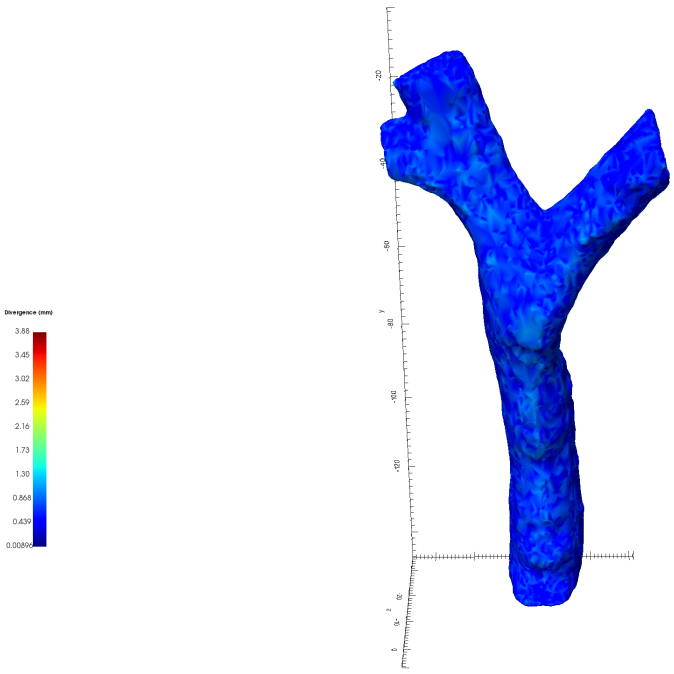

Figure 5.10: Visualization of Mesh Heat Map

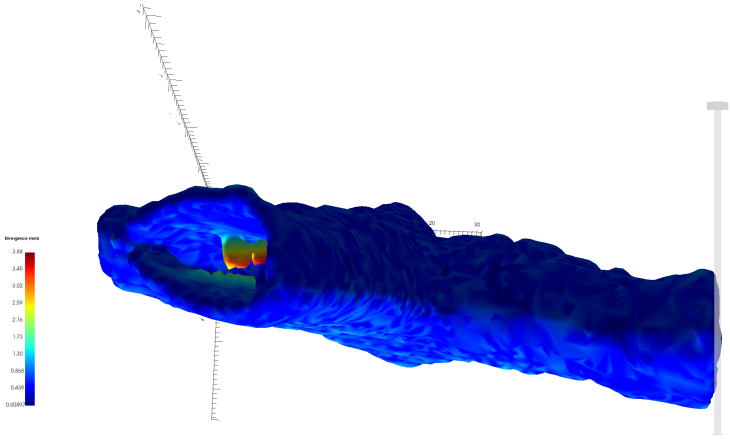

Figure 5.11: Error Region Visualization

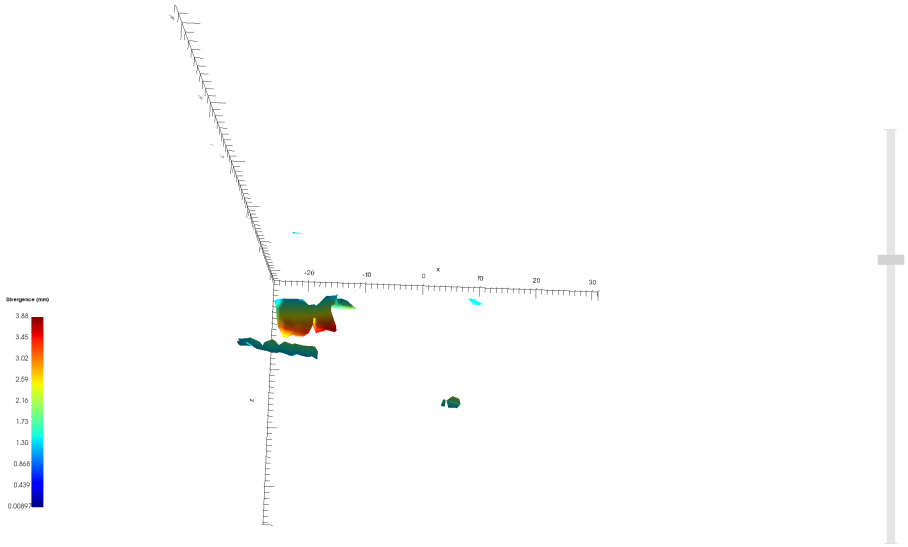

Figure 5.12: Error Isolation

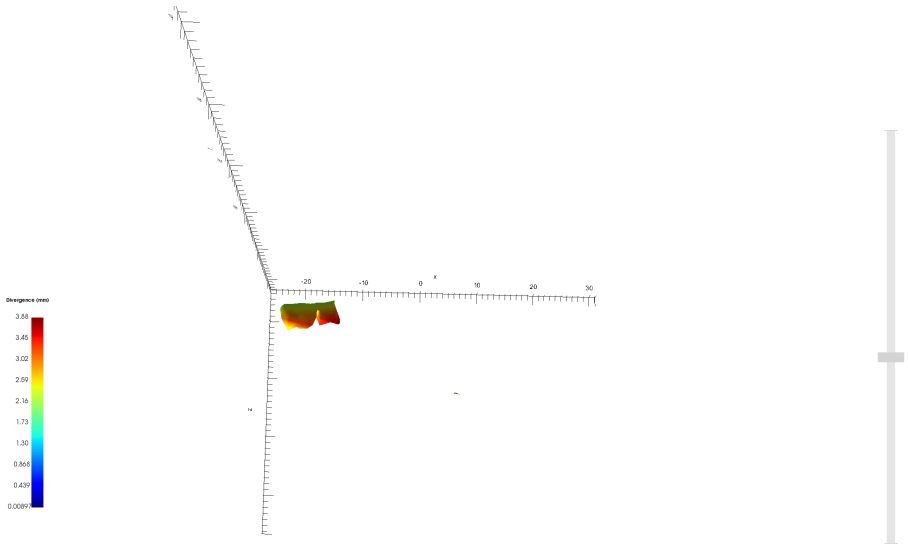

Figure 5.13: Further Error Isolation

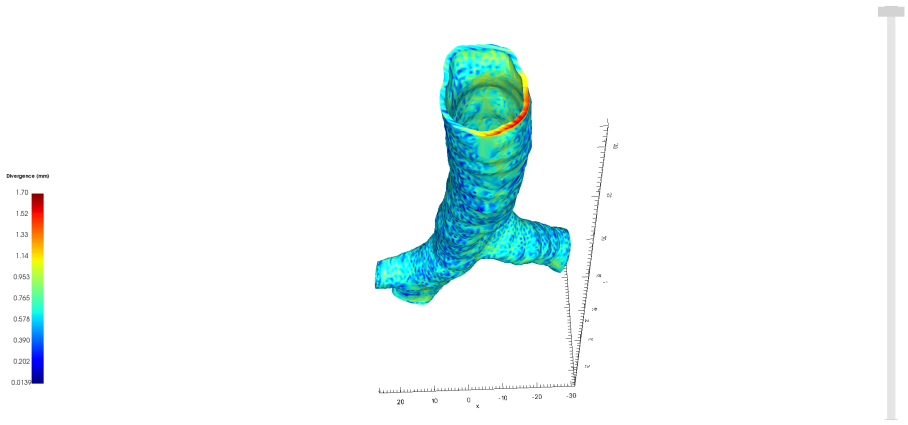

Figure 5.14: Comparing Target Mesh to Source Mesh

5.4.2 Orthopedic Screw Comparison

Next, the 3D model of the orthopedic screw with the hollow internal region was compared to its original. The results are displayed in Figure 5.15.

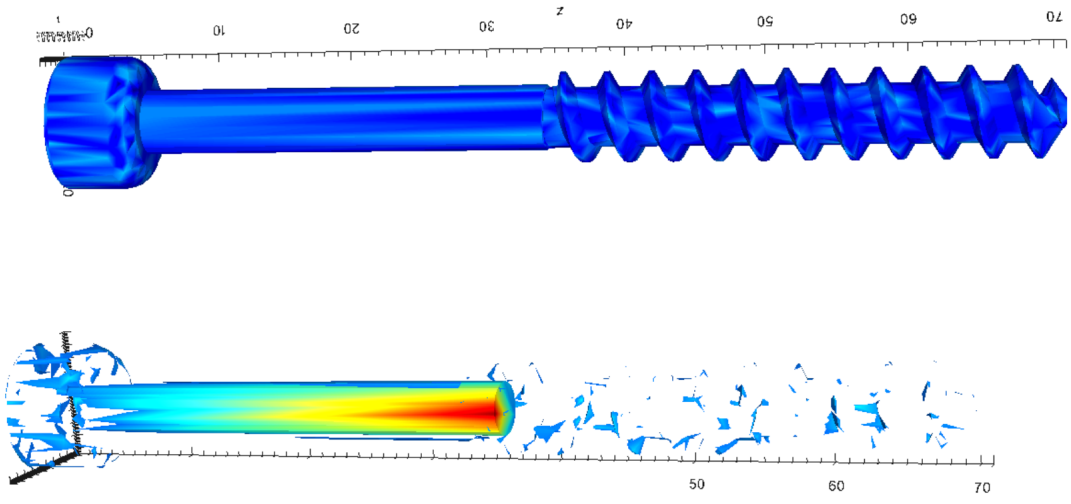

Figure 5.15: Orthopedic Screw Error Visualization

5.4.3 Porous Bone Scaffold Comparisons

Finally, the 3D attack models of the of bone scaffold were compared to their original models, for all three attack model types. Figure 5.16 displays the visual error region isolation produced for the hollow region attack, for spheres of size 2.5 mm.

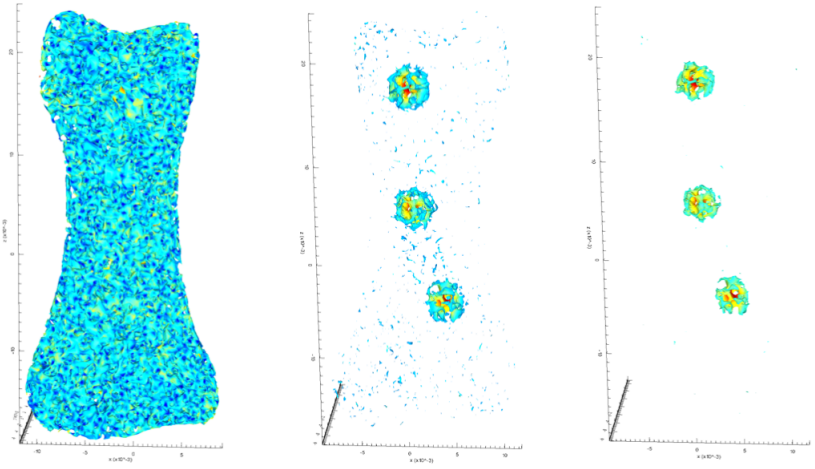

Figure 5.16: 2.5 mm Diameter Hollow Sphere Error Identification

Figure 5.17 displays the visual error region isolation produced for the solid region attack, for spheres of size 2.5 mm.

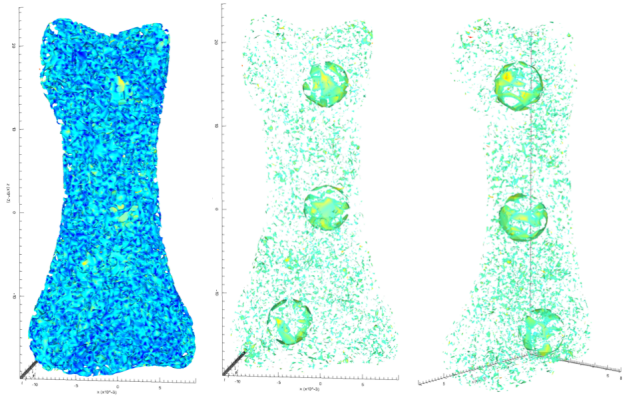

Figure 5.17: 2.5 mm Diameter Solid Sphere Error Identification

Finally, Figure 5.18, shows the visual error isolation for the modified porous region attack, with a modified porous region 3 mm in length.

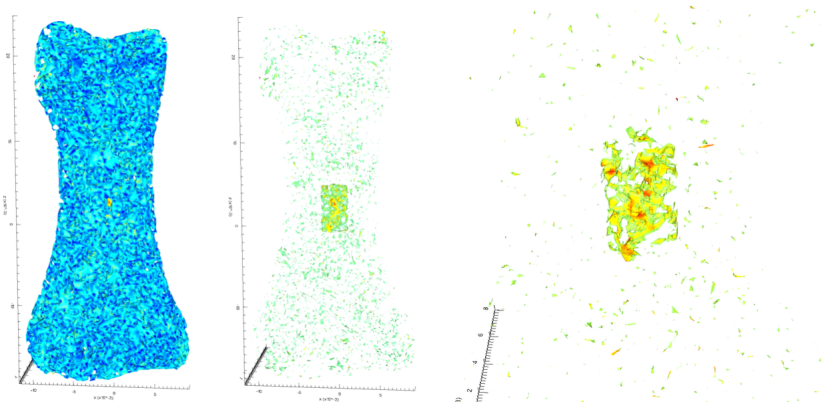

Figure 5.18: Modified Porous Region Error Identification

The modified regions were identifiable for all attack models, except for the added material attack model with the smallest spheres. In this model, three spheres 0.5 mm in diameter were positioned throughout the scaffold. As shown in Figure 5.19, only one of the 0.5 mm spheres was clearly identifiable using the visual error isolation tool. This was fairly surprising since all of the spheres in the 1 mm sphere model (the second smallest) were clearly identifiable, as is shown in Figure 5.20.

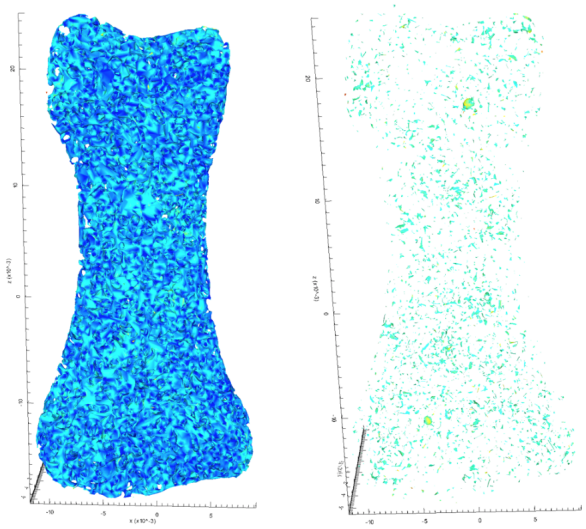

Figure 5.19: 0.5 mm Diameter Solid Sphere Error Identification

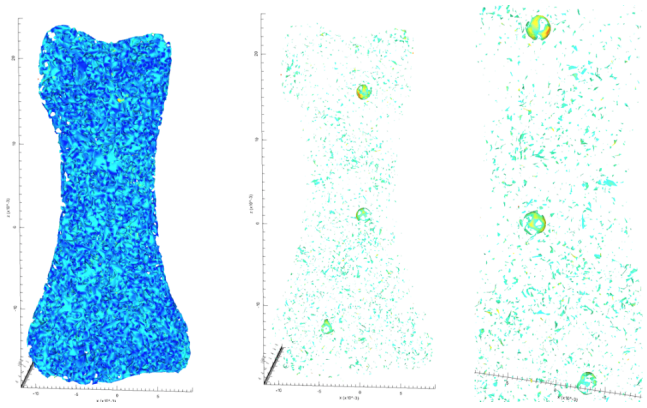

Figure 5.20: 1 mm Diameter Solid Sphere Error Identification

Due to the limits of the sampling procedure, the smallest identifiable part errors are determined by the sampling density when comparing one mesh to the other. Increasing the number of sample points taken from a mesh surface decreases the distance between the sample points and as such, produces a more visually-clean result when comparing meshes. However, for very dense meshes, or for very small errors, the distances between sampled points may be greater than the size of the defects in question, as was the case for the comparison of the added 0.5 mm sphere model shown in 5.19. In order to account for this, the number of sampling points must be increased. However, the required number of sample points becomes exponentially greater as the resolution of the of the defect isolation gets smaller. Given the computational complexity of the distance comparison step, the number of surface samples that can be used serves as a limiting factor.

Chapter 6

Conclusion

Based on the growing use of AM in many industries, combined with the unique security considerations that must be addressed when using this technology, a method for verifying the geometry of 3D printed parts is necessary. In this work, a tool for comparing the geometric similarity between a 3D printed part and its original geometry based off of CT scanning is presented. The tool demonstrated the ability to isolate additive material defects, subtractive material defects, and modifications to geometric features.

The limiting factors in this detection mechanism are the resolution of the scanning images and the sampling limit of each mesh. The resolution of the CT scans depends largely on the scanning machine used. With micro-CT technology, micrometer scale resolutions can be achieved in CT scans. The sampling limit on the other hand depends largely on the computational capacity of the computer used for the analysis. This is because in the distance calculations between the points in both meshes, each point in one mesh is compared to every sample point from the other mesh.

Moving forward, the need for encompassing part verification techniques for AM will only increase. Many traditional verification methods are not suitable for AM applications, as they lack the ability to detect internal defects. Additionally, many traditional cyber-defense strategies are not suitable for AM either. It is not enough to assume the security of these systems or the validity of the parts they produce. This is because many AM parts are used in safety critical systems, and the validity of each part must therefore be ensured.

References

[1] Dicom ps3.6 2020b - data dictionary.

[2] Laminated object manufacturing. *Rapid Prototyping Technology Dekker Mechanical Engineering*, Sep 2001.

[3] Selective laser sintering. *CIRP Encyclopedia of Production Engineering*, page 1095–1095, 2014.

[4] Design and fabrication of powder based binder jetting 3d printer. *International Journal of Recent Trends in Engineering and Research*, 3(9):142–150, 2017.

[5] Cansizoglu, O. and Harrysson, Ola and Cormier, Denis and West, Harvey and Mahale, T. Properties of ti–6al–4v non-stochastic lattice structures fabricated via electron beam melting. *Material Science and Engineering: A*, 492:468–474, September 2008.

[6] Aamer Ahmed, Chris Bonner, and Tejal A. Desai. Bioadhesive microdevices with multiple reservoirs: a new platform for oral drug delivery. *Journal of Controlled Release*, 81(3):291–306, 2002.

[7] Mustafa Alomari, Fatima H. Mohamed, Abdul W. Basit, and Simon Gaisford. Personalised dosing: Printing a dose of one's own medicine. *International Journal of Pharmaceutics*, 494(2):568–577, 2015.

[8] S. Barone, M. Casinelli, M. Frascaria, A. Paoli, and A. V. Razionale. Interactive design of dental implant placements through cad-cam technologies: from 3d imaging to additive manufacturing. *International Journal on Interactive Design and Manufacturing*, 10:105–116, April 2014.

[9] Sofia Belikovetsky, Yosef A. Solewicz, Mark Yampolskiy, Jinghui Toh, and Yuval Elovici. Digital audio signature for 3d printing integrity. *IEEE Transactions on Information Forensics and Security*, 14(5):1127–1141, 2019.

[10] Sofia Belikovetsky, Mark Yampolskiy, Jinghui Toh, Jinghui Gatlin, and Yuval Elovici. dr0wned-cyber-physical attack with additive manufacturing, 2017.

[11] David L. Bourell, Joseph J. Beaman, and Terry Wohlers. History of additive manufacturing. *Additive Manufacturing Processes*, page 1–8, 2020.

[12] Thore M. Bücking, Emma R. Hill, James L. Robertson, Efthymios Maneas, Andrew A. Plumb, and Daniil I. Nikitichev. From medical imaging data to 3d printed anatomical models. *Plos One*, 12(5), 2017.

[13] Jovani Castelan, Lirio Schaeffer, Anderson Daleffe, Daniel Fritzen, Vanessa Salvaro, and Fábio Pinto da Silva. Manufacture of custom-made cranial implants from dicom images using 3d printing, cad/cam technology and incremental sheet forming. *Revista Brasileira de Engenharia Biomédica*, 30:265–273, September 2015.

[14] C Castro, E Sánchez, A Delgado, I Soriano, P Núñez, M Baro, A Perera, and C Évora. Ciprofloxacin implants for bone infection. in vitro–in vivo characterization. *Journal of Controlled Release*, 93(3):341–354, 2003.

[15] Jian-Jun Chen, Wei Liu, Ming-Zhe Li, and Cheng-Tao Wang. Digital manufacture of titanium prosthesis for cranioplasty. *The International Journal of Advanced Manufacturing Technology*, 27:1148–1152, March 2005.

[16] S. R. Chhetri, A. Canedo, and M. A. Al Faruque. Kcad: Kinetic cyber-attack detection method for cyber-physical additive manufacturing systems. In *2016 IEEE/ACM International Conference on Computer-Aided Design (ICCAD)*, pages 1–8, 2016.

[17] P. Choong, M. Dowsey, and J. Stoney. Does accurate anatomical alignment result in better function and quality of life? comparing conventional and computer-assisted total knee arthroplasty. *The Journal of Arthroplasty*, 24:560–569, June 2009.

[18] Mark A. Creager, Joshua A. Beckman, and Joseph Loscalzo. *Vascular medicine: a companion to Braunwalds heart disease*. Elsevier, 2020.

[19] Alekhak Dash and Greggreyc Cudworth. Therapeutic applications of implantable drug delivery systems. *Journal of Pharmacological and Toxicological Methods*, 40(1):1–12, 1998.

[20] A. Dawood, B. Marti, and V. Sauret-Jackson. 3d printing in dentistry. *British Dental Journal*, 219:521–529, December 2015.

[21] David C. Dunand. Processing of titanium foams. *Advanced Engineering Materials*, 6:369–376, June 2004.

[22] Nawfal F. Fadhel, Richard M. Crowder, Fatimah Akeel, and Gary B. Wills. Component for 3d printing provenance framework: Security properties components for provenance framework. *World Congress on Internet Security (WorldCIS-2014)*, 2014.

[23] Navid Farahani, Alex Braun, Dylan Jutt, Todd Huffman, Nick Reder, Zheng Liu, Yukako Yagi, and Liron Pantanowitz. Three-dimensional imaging and scanning: Current and future applications for pathology. *Journal of Pathology Informatics*, 8(1):36, 2017.

[24] Seyed Farid, Seyed Shirazi, Samira Gharehkhani, Mehdi Mehrali, Hooman Yarmand, Simon Hendrik, Cornelis Metselaar, Nahrizul Adib Kadri, and Noor A. A. Osman. A review on powder-based additive manufacturing for tissue engineering: selective laser sintering and inkjet 3d printing. *Science and Technology of Advanced Materials*, 16, June 2015.

[25] Juan Felipe, Isaza Saldarriaga, Santiago C. Vélez, Adolfo C. Posada, Balmore B. Henao, and Carlos A. T. Valencia. Design and manufacturing of a custom skull implant. *American Journal of Engineering and Applied Sciences*, 4:169–174, January 2011.

[26] Food and Drug Association.

[27] Simon Ford and Mélanie Despeisse. Additive manufacturing and sustainability: an exploratory study of the advantages and challenges. *Journal of Cleaner Production*, 137:1573–1587, November 2016.

[28] Matthew Franchetti and Connor Kress. An economic analysis comparing the cost feasibility of replacing injection molding processes with emerging additive manufacturing techniques. *The International Journal of Advanced Manufacturing Technology*, 88:2573–2579, February 2017.

[29] John R. Fredieu, Jennifer Kerbo, Mark Herron, Ryan Klatte, and Malcolm Cooke. Anatomical models: a digital revolution. *Medical Science Educator*, 25(2):183–194, 2015.

[30] Andreas Gebhardt. *Understanding Additive Manufacturing*. Hanser, Munich, 1st edition, 2012.

[31] Ian Gibson, David Rosen, and Brent Stucker. Sheet lamination processes. *Additive Manufacturing Technologies*, page 219–244, 2015.

[32] L. W. Goldman. Principles of ct: Multislice ct. *Journal of Nuclear Medicine Technology*, 36(2):57–68, 2008.

[33] Prasad Guggari. Characterization of mechanical properties of fused deposition modeling manufactured polycarbonate composites.

[34] Kathrin Haberstroh, Kathrin Ritter, Jens Kuschnierz, Kai-Hendrik Bormann, Christian Kaps, Carlos Carvalho, Rolf Mülhaupt, Michael Sittinger, and Nils-Claudius Gellrich. Bone repair by cell-seeded 3d-bioplotted composite scaffolds made of collagen treated tricalciumphosphate or tricalciumphosphate-chitosan-collagen hydrogel or plga in ovine critical-sized calvarial defects. *Journal of Biomedical Materials Research Part B: Applied Biomaterials*, 93B(2):520–530, Nov 2010.

[35] Ola L.A. Harrysson, Omer Cansizoglu, Denis J Marcellin-Little, Denis R. Cormier, and Harvey A. West. Direct metal fabrication of titanium implants with tailored materials and mechanical properties using electron beam melting technology. *Materials Science and Engineering: C*, 28:366–373, April 2008.

[36] Sukjoon Hong. Selective laser sintering of nanoparticles. *Sintering of Functional Materials*, Jul 2018.

[37] L.j. Hornbeck. Digital light processing and mems: an overview. *Digest IEEE/Leos 1996 Summer Topical Meeting. Advanced Applications of Lasers in Materials and Processing.*

[38] Jiang Hsieh. *Computed tomography: principles, design, artifacts and recent advances.* SPIE, 2015.

[39] R. Jeffery, R. Morris, and R. Denham. Coronal alignment after total knee replacement. *The Journal of bone and joint surgery. British volume*, 73:709–714, September 1991.

[40] Cho-Pei Jiang and Yo-Yu Chen. Biofabrication of hybrid bone scaffolds using a dual-nozzle bioplotter and in-vitro study of osteoblast cell. *International Journal of Precision Engineering and Manufacturing*, 15(9):1947–1953, 2014.

[41] Mamta Juneja, Niharika Thakura, Dinesh Kumara, Ankur Gupta, Babandeep Bajwa, and Prashant Jindal. Accuracy in dental surgical guide fabrication using different 3-d printing techniques. *Additive Manufacturing*, 22:243–255, August 2018.

[42] Tomas Kellner. Fit to print: New plant will assemble world's first passenger jet engine with 3d printed fuel nozzles, next-gen materials. Technical report, General Electric, Boston, 2014.

[43] Bryan Kessel. Characterizing and defending against cyber security vulnerabilities in additive manufacturing.

[44] Alaadien Khalyfa, Sebastian Vogt, Jürgen Weisser, Gabriele Grimm, Annett Rechtenbach, Wolfgang Meyer, and Matthias Schnabelrauch. Development of a new calcium phosphate powder-binder system for the 3d printing of patient specific implants. *Journal of Materials Science: Materials in Medicine*, 18:909–916, January 2007.

[45] S. P. Krishnan, A. Dawood, R. Richards, J. Henckel, and A. J. Hart. A review of rapid prototyped surgical guides for patient-specific total knee replacement. *The Journal of Bone and Joint Surgery. British volume*, 94:1457–1461, November 2012.

[46] Bernd Lethaus, Lucas Poort, Roland Böckmann, Ralf Smeets, Rene Tolba, and Peter Kessler. Additive manufacturing for microvascular reconstruction of the mandible in 20 patients. *Journal of Cranio-Maxillofacial Surgery*, 40(1):43–46, 2012.

[47] Xiang Li, Chengtao Wang, Wenguang Zhang, and Yuanchao Li. Fabrication and characterization of porous ti6al4v parts for biomedical applications using electron beam melting process. *Materials Letters*, 63:403–405, February 2009.

[48] C. Liu, Z. Xia, and J.t. Czernuszka. Design and development of three-dimensional scaffolds for tissue engineering. *Chemical Engineering Research and Design*, 85(7):1051–1064, 2007.

[49] R. Liu, Z. Wang, T. Sparks, F. Liou, and J. Newkirk. *Aerospace applications of laser additive manufacturing*. Woodhead Publishing, Cambrdige, 2017.

[50] Angelats Lobo and Ginestra. Cell bioprinting: The 3d-bioplotter^{TM} case. *Materials*, 12(23):4005, Feb 2019.

[51] S.h. Masood. Advances in fused deposition modeling. *Comprehensive Materials Processing*, page 69–91, 2014.

[52] Simone Mastrogiacomo, Weiqiang Dou, John A. Jansen, and X. Frank Walboomers. Magnetic resonance imaging of hard tissues and hard tissue engineered bio-substitutes. *Molecular Imaging and Biology*, 21(6):1003–1019, Jul 2019.

[53] Donald Monkhouse, Chen-Chao Wang, and Charles Rowe. Theriform technology. *Drugs and the Pharmaceutical Sciences Modified-Release Drug Delivery Technology*, page 77–87, Jul 2002.

[54] Samuel Moore, Phillip Armstrong, Todd Mcdonald, and Mark Yampolskiy. Vulnerability analysis of desktop 3d printer software. *2016 Resilience Week (RWS)*, 2016.

[55] Carlos Mota, Dario Puppi, Federica Chiellini, and Emo Chiellini. Additive manufacturing techniques for the production of tissue engineering constructs. *Journal of Tissue Engineering and Regenerative Medicine*, 9(3):174–190, 2012.

[56] Lawrence E. Murr, Sara M. Gaytan, Edwin Martinez, Frank Medina, and Ryan B. Wicker. Next generation orthopaedic implants by additive manufacturing using electron beam melting. *International Journal of Biomaterials*, 2012:245727–245727, August 2012.

[57] L.e. Murr and S.m. Gaytan. Electron beam melting. *Comprehensive Materials Processing*, page 135–161, 2014.

[58] Andriy Myronenko and Xubo Song. Point set registration: Coherent point drift. *IEEE Transactions on Pattern Analysis and Machine Intelligence*, 32(12):2262–2275, 2010.

[59] Samad Nadimi Bavil Oliaei and Behzad Nasseri. 6. stereolithography and its applications. *Additive and Subtractive Manufacturing*, page 229–250, 2019.

[60] Jeong Hun Park, Jinah Jang, Jung-Seob Lee, and Dong-Woo Cho. Three-dimensional printing of tissue/organ analogues containing living cells. *Annals of Biomedical Engineering*, 45(1):180–194, 2016.

[61] Sung Woo Park, Jong Woo Choi, Kyung S. Koh, and Tae Suk Oh. Mirror-imaged rapid prototype skull model and pre-molded synthetic scaffold to achieve optimal orbital cavity reconstruction. *Journal of Oral and Maxillofacial Surgery*, 73(8):1540–1553, 2015.

[62] Michael J. Paulus, Shaun S. Gleason, Stephen J. Kennel, Patricia R. Hunsicker, and Dabney K. Johnson. High resolution x-ray computed tomography: An emerging tool for small animal cancer research. *Neoplasia*, 2(1-2):62–70, 2000.

[63] Norbert J. Pelc. Recent and future directions in ct imaging. *Annals of Biomedical Engineering*, 42(2):260–268, 2014.

[64] Anatoliy Popovich, Vadim Sufiiarov, Igor Polozov, Evgenii Borisov, and Dmitriy Masaylo. Producing hip implants of titanium alloys by additive manufacturing. *International Journal of Bioprinting*, 2:187–193, August 2016.

[65] Leena Kumari Prasad and Hugh Smyth. 3d printing technologies for drug delivery: a review. *Drug Development and Industrial Pharmacy*, 42(7):1019–1031, 2015.

[66] Konda Gokuldoss Prashanth. Selective laser melting: Materials and applications. *Journal of Manufacturing and Materials Processing*, 4(1):13, 2020.

[67] A.a. Rabinstein. Magnetic resonance imaging and computed tomography in emergency assessment of patients with suspected acute stroke: a prospective comparison. *Yearbook of Neurology and Neurosurgery*, 2008:22–24, 2008.

[68] Tanweer Rashid, Sharmin Sultana, and Michel A. Audette. Watertight and 2-manifold surface meshes using dual contouring with tetrahedral decomposition of grid cubes. *Procedia Engineering*, 163:136–148, 2016.

[69] Mason Rice and Sujeet Shenoi. *Critical Infrastructure Protection IX: 9th IFIP 11.10 International Conference, ICCIP 2015, Arlington, VA, USA, March 16-18, 2015, revised selected papers*. Springer, 2015.

[70] Garrett Ryan, Abhay Pandit, and Dimitrios P. Apatsidis. Fabrication methods of porous metals for use in orthopaedic applications. *Biomaterials*, 27:2651–2670, March 2006.

[71] Mika Salmi, Kaija-Stiina Paloheimo, Jukka Tuomi, Jan Wolff, and Antti Mäkitie. Accuracy of medical models made by additive manufacturing (rapid manufacturing). *Journal of Cranio-Maxillofacial Surgery*, 41(7):603–609, 2013.

[72] Md. Sarker and X. B. Chen. Modeling the flow behavior and flow rate of medium viscosity alginate for scaffold fabrication with a three-dimensional bioplotter. *Journal of Manufacturing Science and Engineering*, 139(8), 2017.

[73] R. Singh, P. D. Lee, R. J. Dashwood, and T. C Lindley. Titanium foams for biomedical applications: a review. *Materials Technology*, 25:127–136, July 2013.

[74] Shelly Singh. 3d printing market by offering (printer, material, software, service), process (binder jetting, direct energy deposition, material extrusion, material jetting, powder bed fusion), application, vertical, technology, and geography - global forecast to 2024. Technical report, Markets and Markets, Magarpatta, 2019.

[75] Shelby A. Skoog, Peter L. Narayan Goering, and Roger J. . Stereolithography in tissue engineering. *Journal of Materials Science: Materials in Medicine volume*, 25:845–856, December 2013.

[76] Ian O. Smith and Peter X. Ma. Biomimetic scaffolds in tissue engineering. *Tissue Engineering*, page 31–39, 2010.

[77] P Sprawls. Aapm tutorial. ct image detail and noise. *RadioGraphics*, 12(5):1041–1046, 1992.

[78] Manu Srivastava, Sandeep Rathee, Sachin Maheshwari, and T. K. Kundra. Additive manufacturing processes utilizing material jetting. *Additive Manufacturing*, page 117–130, 2019.

[79] Logan D. Sturm, Christopher B. Williams, Jamie A. Camelio, Jules White, and Robert Parker. Cyber-physical vulnerabilities in additive manufacturing systems: A case study attack on the .stl file with human subjects. *Journal of Manufacturing Systems*, 44:154–164, 2017.

[80] Philip Tack, Jan Victor, Paul Gemmel, and Lieven Annemans. 3d-printing techniques in a medical setting: a systematic literature review. *BioMedical Engineering OnLine*, 15(1), 2016.

[81] Van Thao Le, Henri Paris, Guillaume Mandil, and Daniel Brissaud. A direct material reuse approach based on additive and subtractive manufacturing technologies for manufacture of parts from existing components. *Procedia CIRP*, 61:229–234, March 2017.

[82] Adam Thompson, Donal Mcnally, Ian Maskery, and Richard K. Leach. X-ray computed tomography and additive manufacturing in medicine: a review. *International Journal of Metrology and Quality Engineering*, 8:17, 2017.

[83] Flaviana Trevisan, Francesco andCalignano, Alberta Aversa, Giulio Marchese, Mariangela Lombardi, Sara Biamino, Daniele Ugues, and Diego Manfredi. Additive manufacturing of titanium alloys in the biomedical field: processes, properties and applications. *Journal of Applied Biomaterials & Functional Materials*, 2:57–67, September 2017.

[84] Stefan Tserovski, Simona Georgieva, Radoil Simeonov, Amir Bigdeli, Heinz Röttinger, and Plamen Kinov. Advantages and disadvantages of 3d printing for pre-operative planning of revision hip surgery. *Journal of Surgical Case Reports*, 2019, July 2019.

[85] Herminso Villarraga-Gómez, Ericka L. Herazo, and Stuart T. Smith. X-ray computed tomography: from medical imaging to dimensional metrology. *Precision Engineering*, 60:544–569, 2019.

[86] Guibin Wang, Shicai Zhu, and Xiukui Li. Comparison of values of ct and mri imaging in the diagnosis of hepatocellular carcinoma and analysis of prognostic factors. *Oncology Letters*, Dec 2018.

[87] Richard G. Weekes, Thomas H. Berquist, Richard A. Mcleod, and William D. Zimmer. Magnetic resonance imaging of soft-tissue tumors: Comparison with computed tomography. *Magnetic Resonance Imaging*, 3(4):345–352, 1985.

[88] Jan Witowski, Nicole Wake, Anna Grochowska, Zhonghua Sun, Andrzej Budzyński, Piotr Major, Tadeusz Jan Popiela, and Michał Pedziwiatr. Investigating accuracy of 3d printed liver models with computed tomography. *Quantitative Imaging in Medicine and Surgery*, 9(1):43–52, 2019.

[89] Mingtao Wu and Young Moon. Alert correlation for cyber-manufacturing intrusion detection. *Procedia Manufacturing*, 34:820–831, 2019.

[90] Mingtao Wu, Heguang Zhou, Longwang Lucas Lin, Bruno Silva, Zhengyi Song, Jackie Cheung, and Young Moon. Detecting attacks in cybermanufacturing systems: Additive manufacturing example. *MATEC Web of Conferences*, 108:06005, 2017.

[91] Mark Yampolskiy, Wayne E. King, Jacob Gatlin, Sofia Belikovetsky, Adam Brown, Anthony Skjellum, and Yuval Elovici. Security of additive manufacturing: Attack taxonomy and survey. *Additive Manufacturing*, 21:431–457, 2018.

[92] S. Yang, K.Ff Leong, Z. Du, and C.K. Chua. The design of scaffolds for use in tissue engineering. part i. traditional factors. *Tissue Engineering*, 6:679–689, December 2001.

[93] Shih-Yuan Yu, Arnav Vaibhav Malawade, Sujit Rokka Chhetri, and Mohammad Abdullah Al Faruque. Sabotage attack detection for additive manufacturing systems. *IEEE Access*, 8:27218–27231, 2020.

[94] Xiaoji Zhang, Yuan-Hui Chueh, Chao Wei, Zhe Sun, Jiwang Yan, and Lin Li. Additive manufacturing of three-dimensional metal-glass functionally gradient material components by laser powder bed fusion with in situ powder mixing. *Additive Manufacturing*, 33:101113, 2020.

[95] Qian-Yi Zhou, Jaesik Park, and Vladlen Koltun. Fast global registration. *Computer Vision – ECCV 2016 Lecture Notes in Computer Science*, page 766–782, 2016.

Vita

Nicholas Deily

Degrees B.A. Physics, May 2019
B.S. Mechanical Engineering, May 2020
M.S. Computer Science, May 2020

Cyber-Physical Security in Additive Manufacturing Applications, Deily, M.S. 2020